Graphene nanoplatelet production through non-ionic surfactant-assisted exfoliation of graphite

by

Cameron Scott Giglio

A thesis submitted to the Department of Chemical Engineering

In conformity with the requirements for

the degree of Master of Applied Science

Queen's University

Kingston, Ontario, Canada

(October, 2017)

Abstract

Liquid phase exfoliation of graphite is performed using ultrasonication and shear exfoliation to produce graphene nanoplatelets (GNPs). Ultrasonication is performed using a tip sonicator under power loads ranging from 35-100% amplitude (corresponding to power of 9-36 W) and concentrations of Pluronic® F127 surfactant in water ranging from 1-15 wt%, under batch and sequential addition of surfactant modalities. Shear exfoliation is achieved using a lab scale shear mixer operated with rotor speeds ranging from 1500 rpm to 8000 rpm and Pluronic® F127 concentrations ranging from 1-10 wt%. Ultrasonication exfoliation demonstrated GNP concentrations as high as 3.01 $mg \cdot mL^{-1}$ at 100% amplitude and 15 wt% surfactant concentration. The average particle sizes of the nanoplatelets, were approximately 200-550 nm for all exfoliation methods as estimated through dynamic light scattering (DLS). Transmission electron microscopy (TEM) characterization revealed particle sizes on the order of hundreds of nanometers in lateral dimension. Ultrasonication resulted in few-layer graphene, with thickness ranging from 4-77 nm as measured by Atomic Force Microscopy (AFM) and aspect ratios of 36-96. Shear mixing generated multi-layer graphene, with thickness ranging from 6-11 nm and aspect ratios of 25-72.

Both processes were modeled using dimensional analysis, which revealed that high yields can be achieved beyond specific thresholds of power density input, rotation speed, and surfactant concentration. Based on the results, shear mixing presents itself as a promising method that can be readily scalable above a rotor speed threshold.

Acknowledgements

First and foremost, I would like to thank my supervisors Dr. Aristides Docoslis and Dr. Marianna Kontopoulou for their assistance and guidance through my two years of research. They have taught me a great deal about project management and how to conduct meaningful research, among many other technical and personal aspects. Without them I would still be as lost as I was on my first day of research. I owe them many thanks.

I want to give special thanks to Jennifer Aiello for her help with the research on ultrasonic exfoliation of graphite with anionic surfactants. Her research helped me gather a basis of which to structure my research and justify the use of non-ionic surfactants in the graphite exfoliation system. Thank you for your help.

My parents, as much as I ramble to them, were always there to offer their advice on topics that I barely even understood at the time. They helped me keep my thoughts straight during heavy periods of research and reminded to not forget about the end goal. They pushed me when I pushed back and without them I would not be where I am today. Thank you.

I would like to appreciate my girlfriend, Mallory Minchau, for her undivided attention during my often-long-winded rants about what was ever on my mind. She never complained about my complaints and offered advice whenever possible. She helped me work through difficult times and understand concepts that were giving me trouble. I cannot express my gratitude towards her willingness to help whenever I needed. Thank you so much.

Finally, I must say thank you to the friends I made during my time at Queen's. You all made these last two years very enjoyable and entertaining. Most of all I would like to appreciate my housemates for discussing difficult topics regarding my research while also providing a fun home environment. My housemate Than, thank you for not going to Japan. It meant a lot.

Table of Contents

List of Tables

List of Figures

List of Abbreviations

2D – Two dimensional

3D – Three dimensional

AFM – Atomic force microscopy

b – measure of the intensity of the surfactant adsorption

BET – Brunauer-Emmett-Teller

C – Exfoliated graphite concentration

C_f – Filtrate block copolymer concentration

C_i – Initial graphite concentration

CMC – Critical micellization concentration

CMT – Critical micellization temperature

CTAB – Cetyl trimethylammonium bromide

D – Rotor diameter

DLS – Dynamic light scattering

E_{BE} – Interlayer binding energy

E_{Clv} – Cleavage energy

E_{Ex} – Exfoliation energy

E_S – Surface energy

FLG – Few layer graphene

GNP – Graphene nanoplatelet

GO – Graphene oxide

m^s – Maximum amount of adsorbed surfactant per unit surface area

m^s_2 – Amount of adsorbed surfactant per unit surface area

MLG – Multilayer graphene

N – Rotor speed

NaC – Sodium cholate

NMP – N-methyl-2-pyrrolidone

P – Power density

PDMS - Polydimethylsiloxane

PPO – Polypropylene oxide

PSD – Particle size distribution

rGO – Reduced graphene oxide

rpm – Rotations per minute

SDC – Sodium deoxycholate

SSA – Specific Surface Area

t – Exfoliation time

TEM – Transmission electron microscopy

UV-VIS – Ultraviolet-visible spectroscopy

V – Solution volume

wt% - Weight percent

Chapter 1: Introduction

1.1 Graphene and its Applications

Graphite, much like diamond, is a well-known and commonplace allotrope of carbon. Individual layers of carbon atoms bonded in a hexagonal pattern make up the graphite plane and are referred to as graphene. Graphene is a two-dimensional atomic crystal having thickness of one atomic layer of sp^2 hybridized carbon atoms in a honeycomb assembly. Graphene is a new area of study that has attracted the attention of many research groups due to its strong mechanical strength, high electrical and thermal conductivity, and large surface area [1]. These unique features make graphene a versatile carbon-based material useful for many practical applications such as polymer nanocomposites [2] [3], sensors [4] [5] [6], and nanoelectronics [7] [8]. Nanocomposites containing graphene have gained significant attention, due to their ability to exceed the performance of conventional composites at low loadings. Compared to carbon nanotubes, graphene has a higher surface area to volume ratio, which is favourable for improving polymer composite properties at low filler concentrations. Low loadings coupled with the high mechanical strength of graphene can make materials lighter and stronger for various applications [9] [10]. Additionally, graphene's excellent electrical properties dramatically improve the conductance of polymer based composites.

The high conductance of graphene is highly desirable in applications involving sensors. Conventional hospital sensing devices used for detecting and monitoring human physiological signals are not easy to use, due to their rigidity and poor portability. Polydimethylsiloxane (PDMS) with single wall nanotube films are typically used in the production of electronic skins and have shown high sensitivities, fast response times, and high reusability [4]. Electronic skins

demonstrate excellent heart monitoring and voice recognition capabilities making it useful as a wearable electronic used for early detection of illnesses and voice therapy [4]. While electronic skins have been developed using carbon nanotubes, graphene has been used in the fabrication of other biosensors indicating its potential application as an electronic skin [11] [12].

While the high electrical sensitivity of graphene [13] is advantageous for medical applications, its potential as a supercapacitor has been the focus of a considerable amount of research. The effectiveness of a supercapacitor is dictated by the surface area of the conductors where a larger surface area is better at storing electrostatic charge [1]. Since graphene is an excellent conductor, the specific capacitance of graphene is relatively large and suitable for supercapacitor applications [14] [15] [16]. Supercapacitors are able to gather and hold high amounts of electrical charge in a relatively short amount of time. In addition, they are operable at very low temperatures where many types of electrochemical batteries stop working. Thus, graphene used as a supercapacitor provides ample applications in electronics ranging from short charging time of electric cars to reliability of emergency radios and flashlights.

1.2 Production Methods

The production of graphene is, currently, the limiting factor for commercial application. Many methods have been implemented to produce graphene and can be characterized into two categories: bottom-up and top-down. Bottom-up fabrication of graphene starts with smaller entities and builds them into larger functional structures. The main advantage of bottom-up is the control of resolution since molecular structures are built from discrete units [17]. Thus, the fabrication can be controlled on the atomic level using synthetic chemical techniques. Chemical vapour deposition growth of graphene encompasses heating reagent molecules to a gaseous state

followed by deposition through a chemical reaction onto a nickel or copper substrate [18]. In contrast, epitaxial growth of graphene involves the heating of silicon carbide to extremely high temperatures under ultra-high vacuum. Under these conditions, the silicon molecules sublimate leaving carbon behind in the form of graphene [19]. Both of these techniques are excellent for generating pristine sheets while maintaining the electrical properties of graphene. However, the production rates [20] limit the practical application of bottom-up methods and are generally expensive. Conversely, top-down methods involve the breakdown of graphite or graphite derivatives (e.g. graphene oxide) into graphene sheets using external forces. The main advantage of top-down is the cost effective and high production rate of graphene nanoplatelets (GNPS). Mechanical exfoliation was the first method used to extract graphene from graphite through repeated peeling of scotch tape [21]. The peeling is capable of overcoming the van der Waals forces that hold graphene layers together to form graphite. While this exfoliation method is relatively cheap and can produce pristine graphene, the practicality is not feasible as it is labour intensive. Chemical exfoliation is a promising method for the production of graphene. Colloidal suspensions are generated in a two-step process; first by the reduction of the van der Waals forces through intercalation [22] followed by the exfoliation into modified graphene sheets [18]. This method generates graphene nanoplatelets with many defects found in the form of oxygen based functional groups and requires a reduction process to obtain graphene-like material. However, the final product often contains a small amount of defects which hinders the electrical properties. Finally, liquid phase exfoliation of graphite offers a method for the production of pristine graphene at high concentrations [18]. External forces are generated using ultrasonication or shear mixing to exfoliate graphite into graphene. Careful selection of the solvent, usually in the form of an organic solvent or surfactant solution, is required to disperse and stabilize the

graphene nanoplatelets. However, the exfoliated graphite often ranges from few-layer to multilayer and is not yet controllable.

1.3 Objective and Outline

Liquid phase exfoliation is a promising, cost-effective, and scalable method for the production of graphene nanoplatelets, however the fundamental principles underlying this method are still poorly understood. This thesis will focus on ultrasonication and shear mixing as graphite exfoliation processes, in an aqueous medium, using a non-ionic, poloxamer surfactant. Specifically, the objective of this thesis is to study the effects of process parameters on the concentration and microstructure of graphene nanoplatelets in a cost-effective and potentially scalable process. Two exfoliation methods were implemented; the first utilizes cavitation bubbles formed during ultrasonication whereas the second involves shear forces generated through shear mixing. The size, thickness and concentration of the produced nanoplatelets, as well as the amount of surfactant adsorbed on these nanoplatelets, are studied as a function of surfactant concentration and time.

Chapter 2 is a literature review on the exfoliation processes used in this thesis. The adsorption characteristics of poloxamers and their role in the stabilization of graphene nanoplatelets is also discussed.

Chapter 3 describes the ultrasonication process using a tip sonicator operating under multiple power loads. The effectiveness of surfactant concentration and sonicator amplitude is investigated by various characterization and microscopy techniques. The nanoplatelet concentration, average size, thickness, and amount of adsorbed surfactant is reported.

In Chapter 4, shear forces are generated using a lab bench shear mixer to investigate the effects of surfactant concentration on the properties of the exfoliated graphite. Various rotor speeds are implemented to study the effects on the concentration of graphene nanoplatelets. The scalability of shear mixing is investigated using a dimensional analysis. Chapter 5 summarizes the results of this thesis and provides recommendations for future work.

Appendix A demonstrates a comparison between an anionic surfactant and the non-ionic surfactant used in the studies of this thesis. Three surfactant concentrations are explored using cetyl trimethylammonium bromide (CTAB) and Pluronic® F127. The resulting GNP concentrations are compared.

Appendix B explores the sequential addition of surfactant and compares the results to the batch counterpart. The effectiveness of the new surfactant delivery system is investigated through the same characterization techniques as chapter 3. The GNP concentrations and average particle sizes are described.

Appendix C shows the results of the extinction coefficient experiments which were used in the Lambert-Beer law to determine the GNP concentration of the exfoliated system. Appendix D describes the dimensional analysis process used in the ultrasonication and shear mixing studies. Appendix E and F show the particle size distribution graphs for ultrasonication and shear mixing, respectively.

Chapter 2: Literature Review

2.1 Intrinsic Properties of Graphene

Graphene is a promising material due to its unique mechanical, electrical, and thermal properties. It is made up of pure carbon bound in a sp^2 hybridized hexagonal pattern forming a 2D structure [23] and is described as the building block for all graphitic materials [24]. Due to its 2D structure, monolayer graphene has a theoretical specific surface area of 2630 $m^2 \cdot g^{-1}$ which is much larger than carbon black and carbon nanotubes [25]. Before its discovery, diamond was known to be one of the strongest materials due to the strong and abundant covalent bonds between carbon atoms. However, the structure of graphene has been shown to be extremely strong with breaking strengths up to 42 $N \cdot m^{-1}$ [26].

Due to the bonding structure of carbon, graphene exhibits excellent electron mobility along the hexagonal lattice. Theoretical mobilities have been estimated to be up to 100,000 $cm^2 \cdot V^{-1} \cdot s^{-1}$ and are weakly dependent on temperature. Currently, some semiconductors exhibit electron mobilities as high as 77,000 $cm^2 \cdot V^{-1} \cdot s^{-1}$ at room temperature [24]. Graphene's unique electrical properties originate from the nature of its charge carriers. Typically, the Schrödinger equation is sufficient to describe the electronic properties of materials. However, the Dirac equation better describes the electrical properties due to its charge carriers mimicking relativistic particles. The lone p-orbital of the sp^2 hybridized carbon atoms allows for electrons to move around the lattice at speeds approaching the speed of light. These relativistic velocities generate low energy quasiparticles known as Dirac fermions [27] which can be seen as electrons that have lost their rest mass. The electrons remain in the π^* band (i.e. the anti-bonding region) where the interaction with the π band contains interesting characteristics as a result of half-filled bands. Most often the

bonding and anti-bonding region make contact in a bowl formation whereas in single layer graphene they meet at a point known as a Dirac point and form Dirac cones [28] [29] [30]. This allows the electrons to travel among the various p-orbitals relatively unimpeded owing to the high electron mobility of single layer graphene.

Experimental studies on the thermal conductivity of graphene revealed values as high as 3000 $W \cdot m \cdot K^{-1}$ [31]. In solid materials heat is carried by acoustic phonons and electrons and tends to be dominated by phonons in graphitic materials. The strong covalent sp^2 bonding enables excellent heat transfer through lattice vibrations explaining the dominance of heat transfer by acoustic phonons over electrons in graphene [32]. In combination with excellent electrical properties, graphene is advantageous over other materials as a thermal conductor. The high thermal conductivity lends itself well as an application in electronic devices as a pathway of heat dissipation to a heat sink preventing temperature rises in operating devices [32].

2.2 Binding Forces of Graphene Layers

Graphene layers are held together through van der Waals forces generated by the instantaneous fluctuations of dipoles between two neighbouring graphenes [33]. The formation of stacked layers in graphite can be found in two forms: symmetric and asymmetric (Figure 2.1) [34]. However, the asymmetric stacking is thermodynamically preferred in nature [35].

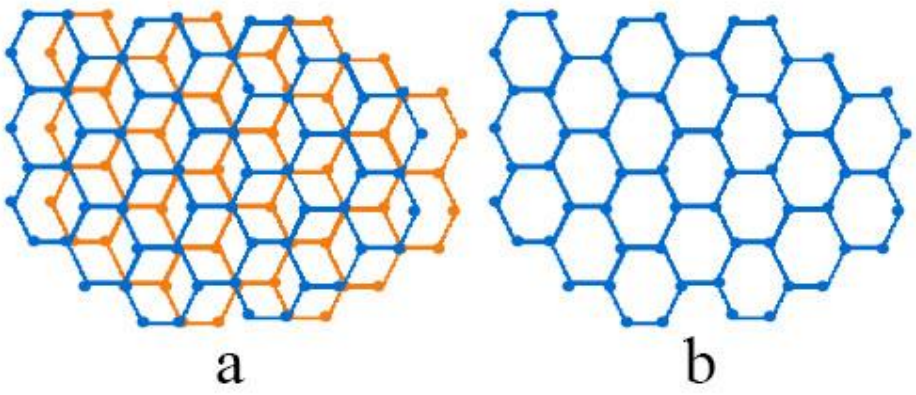

Figure 2.1: Formation of stacked layers in graphene. (a) Asymmetric stacking. (b) Symmetric stacking (bottom layer is fully covered).

Dipole-dipole interactions are inversely proportional to the distance between planes; at large distances they are the dominant force between two graphene sheets. In general, the van der Waals forces keep adjacent graphene sheets in balance through attractive and repulsive forces originating from the Pauli exclusion principle. In metallic or covalent solids (e.g. graphene), the formation of these bonds is driven by the delocalization of electrons along the nearest-neighbour direction [34]. Graphene layers have been theoretically and experimentally measured to have an interplanar distance of ~3.35 Å [34]. In the literature four energies are typically used interchangeably to explain the binding energy between layers in a solid. These energies are referred to as the interlayer binding energy (E_{BE}), the exfoliation energy (E_{Ex}), the surface energy (E_S), and the cleavage energy (E_{Clv}). The interlayer binding forces are quantifiable based on the energy per layer per area required to split the bulk material into widely separated layers (Figure 2.2) [36]. Exfoliation energies can be described as the energy required to form a single layer from the surface of a bulk material [37] and is approximately equivalent to the interlayer binding energy [38]. The surface energy and cleavage are more closely related. The cleavage energy is a

measure of the energy required to divide a crystal into two parts along its basal plane [37] [38] while the surface energy is the energy required to remove a unit of surface through cleavage [38]. It is estimated that the four binding energies can be related to each other through $E_{Ex} \approx E_{BE}$ [38]$\approx 0.85 E_{Clv}$ [36] and $E_{Clv} = 2E_S$ [38]. Experimental results demonstrate cleavage energies of ~0.19 [36]-0.22 $J \cdot m^{-2}$ [39], and binding energies of ~0.17 [36]-0.19 $J \cdot m^{-2}$ [39].

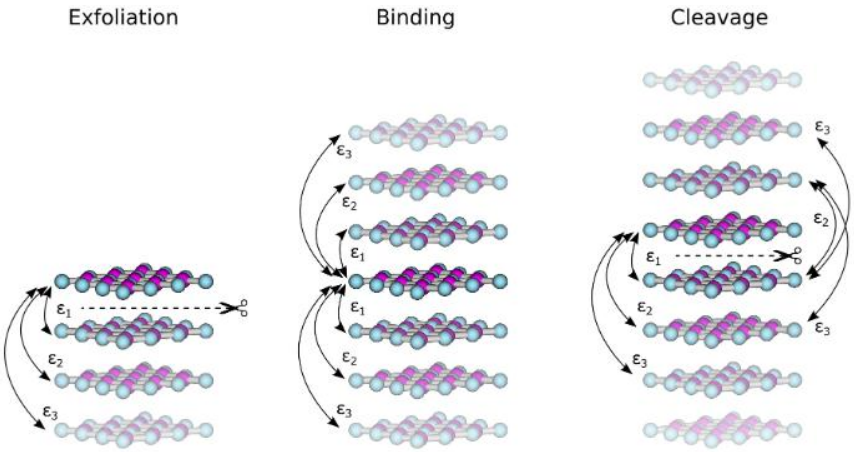

Figure 2.2: Schematic diagram on the classification of the types of interlayer binding in graphite [38].

2.3 Graphene Oxide and Reduced Graphene Oxide

The push towards a high-yield and cost-effective method for graphene production is constantly growing. Covalent modification of graphite to form graphene oxide has proven to produce high-yields presenting itself as a potential method for graphene production. Graphene oxide (GO) is a material consisting of single to few layer carbon sheets bonded to oxidized groups such as hydroxyls and epoxides (Figure 2.3) resulting in their excellent dispersion in aqueous media [3] [40] [41] [42] [43].

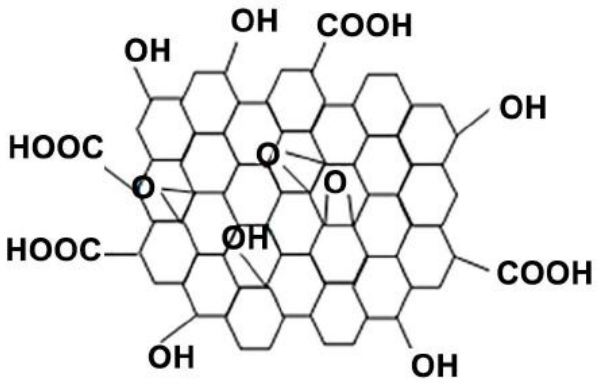

Figure 2.3: A schematic example of the graphene oxide structure [44].

Preparation of graphene oxide from graphite is a simple process obtaining yields as high as 20 wt% with respect to the oxidized graphite [45]. The most common synthesis process of graphene oxide is the modified Hummers' method involving the use of concentrated sulphuric acid and potassium permanganate as an oxidizer [46] [47]. Further modifications of the Hummers' method are possible, such as substituting potassium ferrate for potassium permanganate [48] or adding a small sonication step to aid in exfoliation [44]. However, because of the chemical conversion, graphene oxide has drastically different electrical properties than pristine graphene; changing from electrically conductive to electrically insulating. Further processing is required to convert the electrical properties of GO closer to pristine graphene through either thermal or chemical reduction to form reduced graphene oxide (rGO). However, rGO has a number of disadvantages found in defects, stability, and processing procedure [42] [45] [49] [50]. Reduction is not capable of removing all the oxygen functionalities present in GO, thereby preventing complete conversion to pristine graphene. Therefore, the electrical conductivity of rGO is unable to match their pristine counterparts due to disruption of the π-orbital structure [51] [52] [53] [54]. In addition, due to its more hydrophobic nature, rGO is incapable of maintaining a stable dispersion in aqueous media [49] [50]. This limits the capabilities of rGO as a

strengthening material in polymers, due to an uneven dispersion of rGO within the material. Lastly, processing times can last 2-4 days [45] [49] to convert graphite to rGO, severely handicapping the production rate. The processing procedure is not desirable as the production and chemical reduction of GO requires many harmful chemicals [45] [49] [55] while thermal reductions require high operating temperatures (≈1000 °C) [43] [55] [56].

2.4 Ultrasonication and Liquid Phase Exfoliation

Liquid phase exfoliation of graphite was first carried out in organic solvents such as N-methyl-pyrrolidone (NMP) and dimethylformamide by Coleman *et al.* [40]. The dispersion of carbon nanotubes in organic solvents [57] was the driving force behind Coleman's work. Liquid phase exfoliation of graphite is advantageous over other methods such as chemical vapour deposition and mechanical exfoliation due to its simplicity and avoidance of high vacuum or temperatures. In addition, some methods of liquid phase exfoliation have shown good potential to be scaled up to an industrial level [58] [59]. However, there are a few challenges associated with liquid phase exfoliation, such as re-aggregation of graphene sheets, production of range of monolayer to multiple layer graphene, and dispersion concentration.

Ultrasonication is an effective processing method and has the potential to produce monolayer to few-layer graphene at relatively high graphene concentrations [54] [60] [61] [62]. The waves produced from ultrasound can be classified into four different categories: longitudinal, shear, surface, and plate, which depend on the direction of propagation. The frequency of the sound waves dictates the category of ultrasound separating into three categories: power ultrasound (20-100 kHz), high frequency ultrasound (100 kHz-1 MHz), and diagnostic ultrasound (1-500 MHz). Typically, power ultrasound is used to induce physical or chemical changes in system through

generation of cavitation bubbles [63] [64]. As the ultrasonic waves propagate through a medium, compressions and rarefactions exert positive and negative pressures that push and pull molecules. During rarefaction, microbubbles begin to form and grow with each cycle until they reach an unstable state and implode generating powerful shockwaves [65] [66] [67]. The use of ultrasonication for the liquid phase exfoliation of graphite has been a promising method for producing graphene at low costs [68] [69] [70]. The cavitation effect produces normal and shear forces that act on graphite. Under the intense forces, exfoliation is induced on graphite causing it to separate into graphene layers.

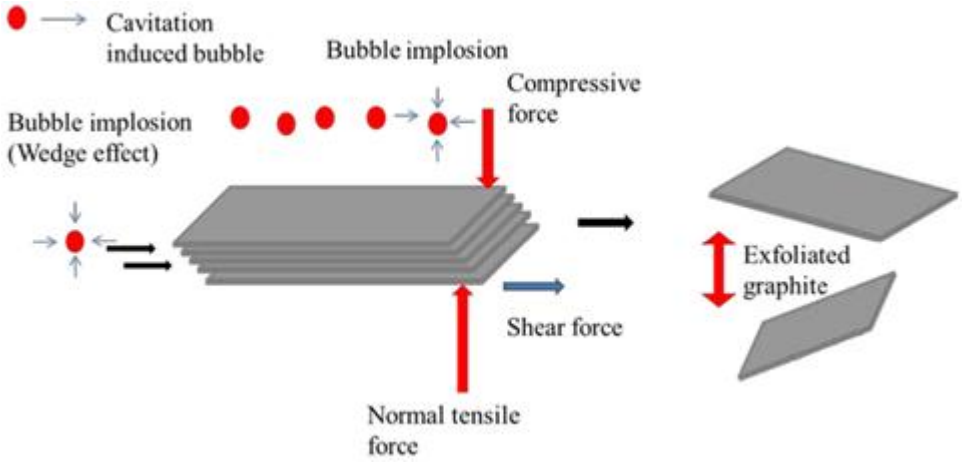

Figure 2.4: Schematic of the exfoliation process induced by bubble cavitation during ultrasonication [71].

The result of exfoliation depends on the power of ultrasonication, the liquid medium used to disperse graphene nanoplatelets, and the degree of subsequent centrifugation. Suitable liquid media are chosen to provide an environment that allows for stable dispersions of graphene produced during sonication. Centrifugation is a post exfoliation process that removes large and unstably dispersed particles or aggregates [70].

2.5 Choice of Dispersion Medium in Liquid-Phase Exfoliation

The surface tension of the liquid medium plays a significant role in exfoliation and dispersion stability through interactions with graphene. Ideally, the liquid would overcome the van der Waals forces between graphene layers by substantially reducing the energetic cost required to separate the layers. This energy balance is expressed as the enthalpy of mixing, which is dependent on the graphene and liquid surface energy [72]. Thus, liquids with surface energies similar to graphene will reduce the energy cost of exfoliation and facilitate dispersion. It has been demonstrated that liquids with surface energies between 40-50 $mJ \cdot m^{-2}$ [40] are the most suitable for graphene exfoliation.

The use of organic liquids or aqueous solutions containing surfactants as a liquid medium must be selected based on the various advantages and disadvantages of both approaches. Organic liquids create a stable environment for suitable graphite exfoliation and graphene suspensions, because their surface energies are more favourable. However, they are typically toxic with high boiling points making disposal more difficult [70]. On the other hand, surfactants in aqueous solutions are more environmentally friendly while producing comparable concentrations of graphene to solvent exfoliation [60] [61] [73]. The disadvantage of using surfactants over organic liquids is due to the adsorption of surfactant onto the graphene surface. While the adsorption process prevents re-aggregation of graphene sheets, an extra processing step is required to remove adhered surfactant before the graphene can be used as intended.

2.6 Poloxamers

Poloxamers are tri-block copolymers that consist of a central hydrophobic block made of polypropylene oxide connected to two hydrophilic blocks made of polyethylene oxide (Figure

2.5). Since the length of the polymer chains can be selected, various types of poloxamers exist and follow a general naming system. Generally, poloxamer names begin with the letter P followed by three digits where the first two digits (multiplied by 100) represent the approximate molecular weight and the last digit (multiplied by 10) represents the percentage of polypropylene oxide content [74]. However, poloxamers are usually called by the tradename "Pluronic" (BASF) and follow a different naming convention. These tradenames begin with a letter to define the physical state at room temperature (L for liquid, P for paste, and F for solid) and end in two or three digits. The first digit (or the first two for a three digit suffix) indicates the approximate molecular weight (multiplied by 300) of the hydrophobic block and the last digit (multiplied by 10) indicates the percentage of polyethylene oxide content [75]. Poloxamers are often used as surfactants, emulsifying agents, solubilizing agents, and dispersing agents [76].

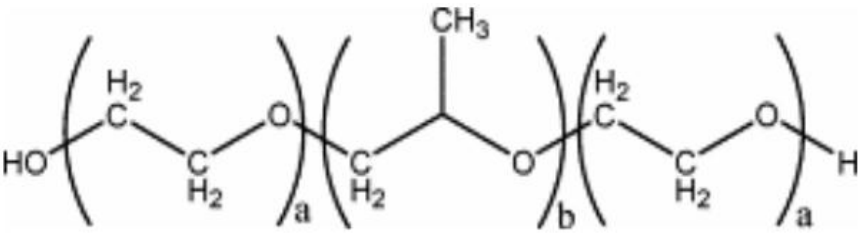

Figure 2.5: General molecular structure for poloxamers [76].

Poloxamers are promising surfactants producing high graphene yields. For example, Guardia *et al.* demonstrated highly concentrated dispersions of graphene with non-ionic surfactants achieving concentrations as high as ~1 $mg \cdot mL^{-1}$ using Pluronic® P123 after 2 hours of bath sonication [77]. Sun *et al.* showed that Pluronic® F127 produced comparable graphene concentration to other non-ionic surfactants [61] while Notley achieved excellent graphene concentrations from graphite exfoliated in Pluronic F108 [62]. The mechanism of liquid-phase graphene exfoliation involves hydrophobic and hydrophilic interactions and utilizes the amphiphilic properties of surfactants. Graphene is hydrophobic in nature; this promotes adhesion

between the hydrophobic portions in surfactant molecules to graphene surface. Conversely, the hydrophilic portions of the surfactant molecules allow for dispersion due to its attraction with water molecules. Thus, the surfactant acts an encapsulating shell stabilizing the graphene by preventing re-aggregation through hydrophobic interactions, while enabling stable dispersions through hydrophilic interactions. Above the critical micellization concentration (CMC), micelles act as the encapsulating shell (Figure 2.6).

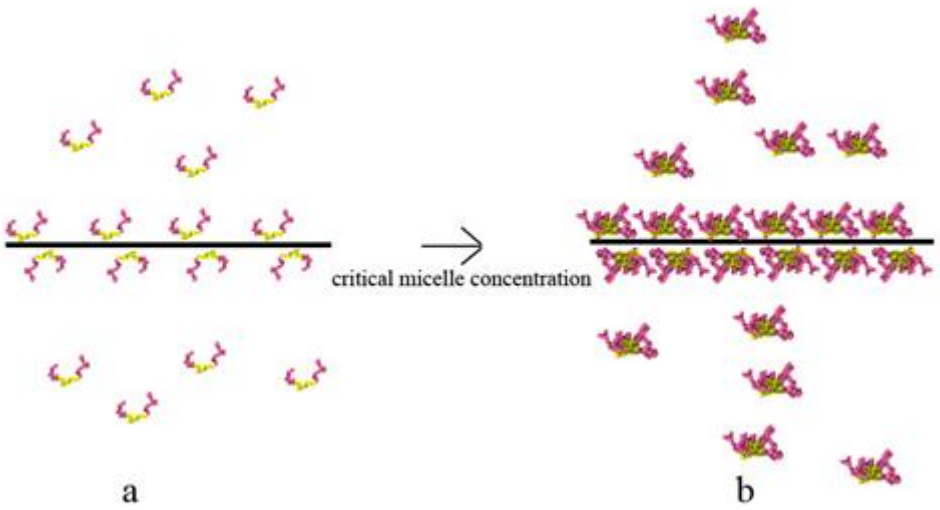

Figure 2.6: Schematic of surfactant adsorption in aqueous media. (a) Adsorption of unimers below critical micellization concentration. (b) Adsorption of micelles above critical micelle concentration [78].

The colloidal stability of dispersed graphene sheets is largely dependent on the amount of adsorbed surfactant and the hydrodynamic thickness of the adsorbed layer [79]. Langmuir adsorption isotherms of many poloxamers onto carbon black have been reported in literature where a plateau region exists at concentrations much smaller than the critical micellization concentration (CMC) [80]. Pluronic® F127 follows the same trends where the isotherm reaches a plateau below CMC when adsorbing onto carbon black [79].

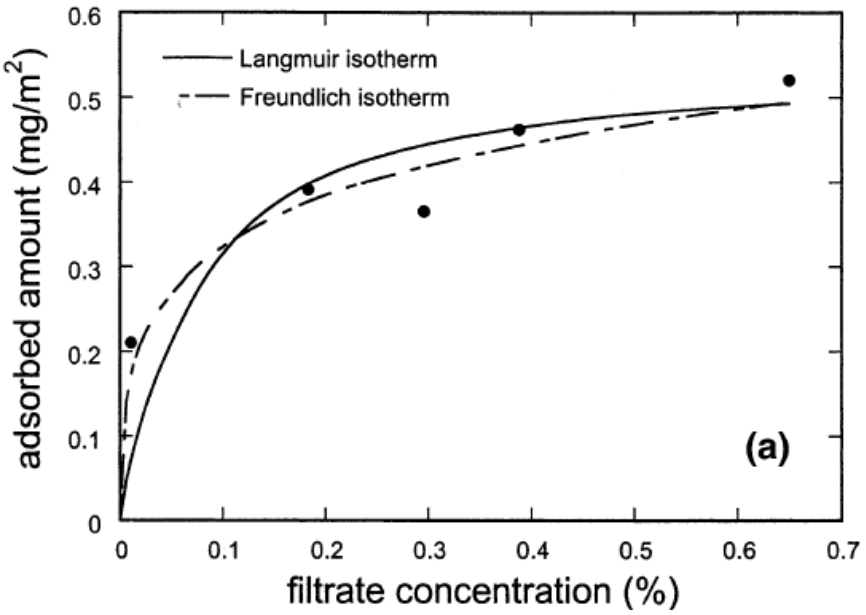

Figure 2.7: Two adsorption isotherms of Pluronic® F127 onto carbon black at 24 °C fitted using Langmuir and Freundlich equations [79]. Surfactant concentrations were tested in the range of 0.1-1 wt%.

Langmuir isotherms carry the assumption of monolayer adsorption indicating that below CMC Pluronic® F127 adsorbs as a monolayer. Therefore, at conditions where the monolayer assumption applies, important adsorption parameters can be determined through the following empirical equation:

$$\frac{C_f}{m_2^s} = \frac{1}{m^s b} + \frac{C_f}{m^s} \quad (1)$$

where C_f is the filtrate block copolymer concentration, $m^s{}_2$ is the amount of adsorbed surfactant per unit surface area, m^s is the maximum amount of adsorbed surfactant per unit surface area, and b is a measure of the intensity of the surfactant adsorption. Thus, with a surface area of 30 $m^2 \cdot g^{-1}$ for carbon black the surface area per molecule of adsorbed Pluronic® F127 is 4.3 nm^2 [79]. Similar studies of the adsorption of Pluronic® F127 onto polystyrene nanoparticles of

various sizes reported similar surface area coverage per molecule [81]. Below the critical micellization temperature (CMT), the layer thickness at 0.01 wt% Pluronic® F127 (7 nm) is smaller than 1 wt% Pluronic® F127 (19.6 nm) and is believed that the block copolymer may not pack tightly at lower concentrations. This effects the polymer conformation such that the hydrophilic chains do not extend as far, thereby decreasing the adsorbed layer thickness. Above CMC, when micelles begin to form, the layer thickness was observed to increase for both 0.01 wt% and 1 wt% Pluronic® F127 surfactant concentrations from 7 to 13.3 nm and 19.6 to 22 nm, respectively. Furthermore, above CMC (or CMT), Pluronic® F127 micelles tend to associate with one another and this may lead to multilayer formation, further increasing the layer thickness [79]. Thus, at high Pluronic® F127 concentrations it is possible to experience larger quantities of surfactant associated with a single adsorbent particle.

2.7 Shear Mixing and Scale-up

Solution based exfoliation of graphite tends to result in high graphene concentrations containing high amounts of defects, or low concentrations with low levels of defects. Sonication of graphite in a stabilizing solvent results in high concentrations of defect-free graphene but is typically exfoliated in volumes of 10-100 mL. Literature studies have shown production rates lower than 0.4 $g \cdot h^{-1}$ coupled with relatively low defect content measured by Raman D/G intensity ratios [54] [82] [83] [84] [85] [86] [87] [88]. These studies were performed on a lab-scale; sonication processes have limited scalability which makes it difficult to increase production rates. Shear mixing offers the potential for large scale opportunities and is already used to disperse nanoparticles in liquids [89]. Additionally, exfoliation of graphite or layered materials that incorporates shear mixing has been demonstrated in the literature. However, intercalation is required to weaken the interlayer binding strength before exfoliation can occur [90] [91] [92].

While the exfoliation process is faster and easier after intercalation, the rate limiting step is shifted to intercalation and scale-up is more difficult to achieve. For scale-up to be possible, graphite should be exfoliated using shear mixing without any pre-treatments. Based on power densities compared to ultrasonication [93] (where power densities are >1500 $W \cdot L^{-1}$), shear mixers deliver low levels of power to the system indicating that exfoliation would likely not occur at an appreciable rate. However, Paton *et al*. has demonstrated a method for the shear exfoliation of graphite that produces graphene nanoplatelet concentrations in NMP and sodium cholate (NaC) solutions comparable to sonication [58]. In addition, the shearing process was shown to be scalable to industrial levels producing large amounts of defect-free graphene. Shear mixers generally consist of a controllable motor unit which is used to drive a rotor/stator apparatus. Typical lab bench mixers offer rotation speeds ranging from 0-8000 rpm and are effective with mixing volumes up to 12 L (Figure 2.8).

Figure 2.8: A Silverson high-shear mixer (Model: L5M-A) exfoliating a graphite dispersion [58].

During mixing, the rotation of the rotor acts as a pump drawing in the solvent and unexfoliated graphite. In the rotor, centrifugal forces drive the particles to the boundary between the rotor and stator. As the solution moves outwards at high velocity, large shear forces are applied to the graphite particles before passing through the perforations in the stator and back into the main solution (Figure 2.9). Constant rotation of the rotor results in the exfoliation of graphite with the aid of shear forces.

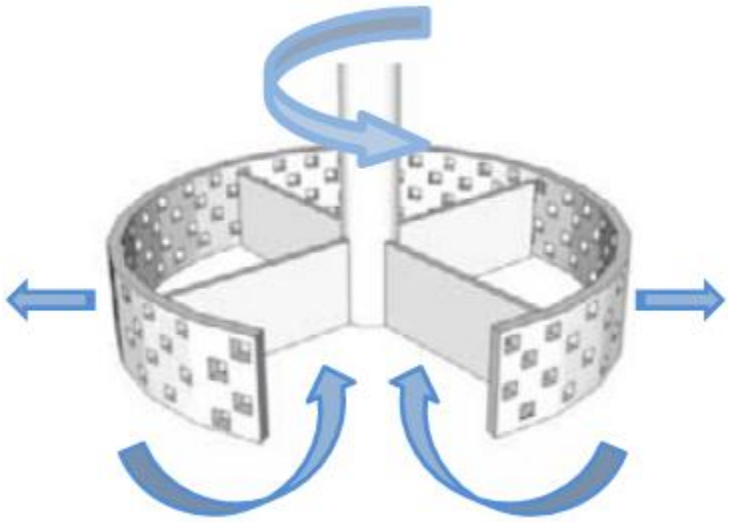

Figure 2.9: Schematic illustration of the operation of the rotor and stator [58].

Initially, it was believed that localized and high turbulent regions were responsible for the exfoliation of graphite. Paton *et al.*, showed that graphene dispersions were produced not only at high Reynolds numbers (turbulent flow) but also at low Reynolds numbers, where the system transitions from laminar to turbulent flow [58]. Dispersons of graphite were shear mixed in a Couette setup under laminar flow conditions to prove turbulence is not a factor in the production of graphene. TEM images confirmed that graphene was produced where the concentration increased with time. Paton *et al.* discovered that a minimum shear rate of ~10^4 s^{-1} was required to

produce graphene. At this shear rate in a Couette setup, laminar flow regimes were still maintained showing that turbulence is not needed for the exfoliation of graphite [58].

Chapter 3: Exfoliation via Ultrasonication

3.1 Introduction

Since the first extraction of a single layer from bulk graphite, graphene has gained significant interest from researchers in an effort to exploit its many great physical properties. Most notably, graphene carries high electrical, mechanical, and thermal properties and acts as an excellent charge carrier [1] or as a strengthening material in polymer composites [2] [3]. These properties are desirable for industrial applications to make better electronic systems or strong, lightweight plastics. Graphene can be produced using bottom-up or top-down methods. Bottom-up approaches (e.g. chemical vapour deposition) allow for better control of the thickness and size of graphene sheets, but tend to be expensive. Top-down methods are more cost-effective, and potentially scalable, and are therefore more favourable for industrial purposes. These methods typically generate mixtures of pristine single and multilayer graphene sheets [17] [18] [94] [95]. Common methods of top-down graphene production are chemical conversion of graphite to graphene oxide (GO) followed by reduction to reduced graphene oxide (rGO) [42] [43] [50], mechanical exfoliation [21] [96], and liquid phase exfoliation of graphite [54] [68] [95].

Liquid phase exfoliation of graphite offers many advantages due to its simplicity and ease of use. A plethora of liquid media can be used in graphite exfoliation: organic solvents [54] [97] [98], or aqueous solutions of ionic [61] [99] or non-ionic surfactants [61] [62] have been employed to produce appreciable amounts of graphene. Surfactant-assisted graphene exfoliation is among the most promising methods for producing highly concentrated graphene dispersions. Surfactant based liquid phase exfoliation is advantageous, as higher concentrations can be achieved in a short time period [61] compared to organic solvents. In addition, surfactant assisted exfoliation is

an environmentally benign method of graphene production due to the use of aqueous solvents. One disadvantage of the surfactant assisted exfoliation, however, is the required removal of surfactant prior to further processing of the exfoliated material. Fortunately, surfactants can be removed by heating the exfoliated mixture, as they typically disintegrate at low enough temperatures [100] to avoid changes in the structure or chemical composition of graphene [101] [102] [103].

While surfactant assisted exfoliation has been researched extensively it is important to note differences in the effects of ionic and non-ionic surfactants on graphene stabilization [88]. Stabilization from ionic surfactants is the most well understood and is associated with electrostatic repulsion. The surfactant tails can adhere to the non-polar graphene surface through van der Waals forces leaving the head groups to disassociate in aqueous liquids. Thus, the graphene flakes are effectively charged causing adjacent surfactant-coated flakes to repel. Non-ionic surfactants stabilize graphene flakes in a different manner as no charge is present for electrostatic repulsion. Like ionic surfactants, the hydrophobic portion adheres to the graphene surface through van der Waals forces, while the hydrophilic chains protrude into the aqueous media. When two surfactant-coated flakes approach each other the hydrophilic chains on the flakes begin to repel each other through steric repulsions [88].

Various studies have been performed to compare ionic to non-ionic surfactant systems on the graphene flakes produced under identical conditions. Most non-ionic surfactant systems perform very well, often providing higher graphene concentrations and better stability [61] [62] [73] [77]. Among non-ionic surfactants, poloxamers have been proven to be quite effective in producing high graphene concentrations in water; yet a very small portion of the available poloxamers has been investigated. Guardia *et al*. demonstrated concentrations as high as ~1 $mg \cdot mL^{-1}$ using

Pluronic® P123 after 2 hours of bath sonication [77]. Sun *et al*. showed that Pluronic® F127 produced comparable graphene concentration to other non-ionic surfactants [61], while Notley obtained excellent graphene yields through sequential addition (85%) of Pluronic® F108 and F127 [62]. Sun *et at.* and Notley showed that Pluronic® F127 demonstrated high performance compared to other surfactants. In appendix A, a preliminary investigation was conducted for this thesis to study the effectiveness of graphite exfoliation in an anionic surfactant using cetyl trimethylammonium bromide (CTAB). It was shown that Pluronic® F127 provided a better environment for the exfoliation of graphite; influencing the choice of surfactant. The literature results provide a promising route for the production of graphene. However, these studies lack full characterization of the graphene platelets choosing to focus mostly on graphene concentration, rather than the properties of the resulting product. In addition, the poloxamer surfactant concentration was kept constant around critical micellization concentrations (CMC) with little research conducted below and above CMC.

In this work, a detailed study is conducted on the effect of a wide-range of operating conditions and Pluronic® F127 concentrations on the yield and properties of the resulting GNPs. The acquired data and modelling are used to propose the mechanism underlying the ultrasonic-assisted exfoliation of graphite. By using tip sonication high concentrations of GNPs can be dispersed and stabilized in Pluronic® F127-water systems in short periods of time. Finally, the data demonstrates that two mechanisms are responsible for the exfoliation of graphite, where a transition between mechanisms is marked at specific sonicating conditions.

3.2 Experimental Section

3.2.1 Materials

Natural graphite powder (purity 95% and 80 mesh) was supplied by Eagle Graphite and purified (99%) with anhydrous ethyl alcohol and acetone. Pluronic® F127 was purchased from Sigma Aldrich and used as received. Milli-Q quality water was used in all of the experiments.

3.2.2 Methods

Graphite (G) was exfoliated using a Microson Ultrasonic Cell Disruptor equipped with a 3 mm diameter sonicating tip. Surfactant concentrations ranging between 0 to 15 wt% were used for the exfoliation process and prepared by dissolving Pluronic® F127 in Milli-Q water to a total volume of 60 mL. Since the dissolution of Pluronic® F127 in water occurs more readily at lower temperatures, the mixture was left to equilibrate for 12 h at 4 °C. Graphite powder (5 wt%) was added to the surfactant solution and stirred until adequately mixed. The graphite-surfactant solution was placed in a temperature controlled bath to maintain temperature at approximately 20 °C (room temperature). A stir bar was placed at the bottom of the beaker to ensure better mixing. Graphite exfoliation was initiated after lowering the sonicating tip halfway into the solution volume and setting the amplitude between 35 to 100% on the digital display (corresponding to 9-34 W). The solution was left to exfoliate for 4 hours with samples taken in 1 hour intervals (3 mL). These samples were centrifuged at 1800 g for 30 minutes and the supernatant was used for characterization through UV-VIS spectroscopy and DLS.

3.2.3 Instrumentation and Analysis

UV-VIS spectroscopy was performed on a Varian Cary 100 Scan spectrophotometer. The selected wavelength range was from 400 to 800 nm and the cuvette path length was 0.01 m. The absorbance was converted to concentration using the Lambert-Beer law. The supernatants of the centrifuged samples were diluted 10-20 fold with Milli-Q water to ensure the absorbance was within the instrument's range.

The extinction coefficient used in these experiments was analytically determined using the Lambert-Beer law with two different methods. First, the absorbance of a known volume was measured using UV-Vis and sequentially dried using a vacuum oven. After drying, the adhered surfactant was removed in an inert atmosphere using TGA and the mass of the dry material was measured. Thus, the concentration of the GNPs was determined by dividing the mass of the dry material by the sample volume. Plotting the absorbance against the nanoplatelet concentration provided the extinction coefficient as the slope of the trend line. In the second method, a known mass of dry, surfactant free material was dispersed in a known volume of NMP. After, the absorbance of the solution was measured using UV-Vis and then plotted against the concentration similar to the previous method. Both methods were in agreement and were averaged to produce an extinction coefficient of 732 $mL \cdot mg^{-1} \cdot m^{-1}$ (λ=660 nm). This is lower than results reported in literature [54] [104] [105] [106], though the extinction coefficient appears to be dependent on the system in which the nanoplatelets were exfoliated [107].

The supernatant samples were further diluted (15-fold) with Milli-Q water and estimates of the particle size distribution of the GNPs were obtained through Dynamic Light Scattering (DLS) measurements, using a Malvern Instruments Zetasizer Nano ZS (λ=633 nm). The polydispersity

index (PdI) in DLS measurements describes the width of a particle size distribution and is calculated from a Cumulant analysis [108]. Thus, true monodisperse solutions inherently have PdI values of 0. However, the classification of monodisperse ranges from 0.0-0.1 whereas polydisperse ranges from 0.1-0.7 [109]. Values > 0.7 indicate samples that are not suitable for DLS [108]. Data obtained through DLS, however, must be interpreted with caution as the reported particle size, calculated from the Stokes-Einstein equation, is that of the spherical equivalent of GNP. Furthermore, the DLS intensity averages are affected more by larger particles than smaller particles. Thus, it must be taken into account that the larger particles will have a greater effect on the particle size distribution when interpreting the PdI.

Thermogravimetric analysis was carried out using a Q500 TGA instrument. Prior to thermogravimetric analysis, the suspensions were filtered using a 0.2 μm pore size Sterlitech Nylon membrane and washed to remove any excess surfactant. The powder was collected and sequentially dried in a vacuum oven at 60 °C for 12h. Samples were heated from room temperature to 400 °C at 20 °C·min^{-1} under a 50 mL·min^{-1} nitrogen gas flow. Isothermal conditions were maintained at 400 °C for 45 minutes before ramping up to 450 °C at 20 °C·min^{-1} to ensure all of the surfactant was degraded.

BET measurements were conducted using an Autosorb-1 by Quantachrome instruments to obtain the specific surface area of the graphene platelets. Samples obtained from TGA were degassed at 300 °C for 4 h and then analyzed using multipoint BET physisorption with nitrogen relative pressures (0.1-0.3 at 77 K).

TEM images were obtained using a Hitachi H-7000 instrument operated at 75 kV. GNPs in the form of dry powder were first dispersed in NMP at 0.1 wt% using an ultrasonic bath for 1.5 h. The sample was then deposited on 300 mesh copper grids and dried before analysis.

AFM measurements were performed using a Veeco Di NanoScope llla AFM, with an AppNano ACT N-type silicon probe (force constant k=37 $N \cdot m^{-1}$, radius of curvature=6 nm, resonance frequency f=300 kHz) in tapping mode. The samples were prepared by spraying the GNP-NMP dispersion described above onto an oxidized silicon wafer. To prevent "ring" effects, the silicon wafers were placed on a hot plate during spray coating, to increase the NMP evaporation rate.

3.3 Results

3.3.1 Effects of time, sonication power, and surfactant concentration on exfoliation performance

Exfoliations were carried out for a total sonication time of 4 h, at various amplitudes and surfactant concentrations. The concentration of exfoliated GNPs increased proportionally with time, for all surfactant concentrations, and at all amplitudes (representative data shown in Figure 3.1(a) and Figure 3.1(b)). Figure 3.1(b) shows a dramatic increase in GNP concentration at 100% amplitude and at surfactant concentrations higher than 10 wt% F127. These differences are noticeable from the beginning of the sonication experiments.

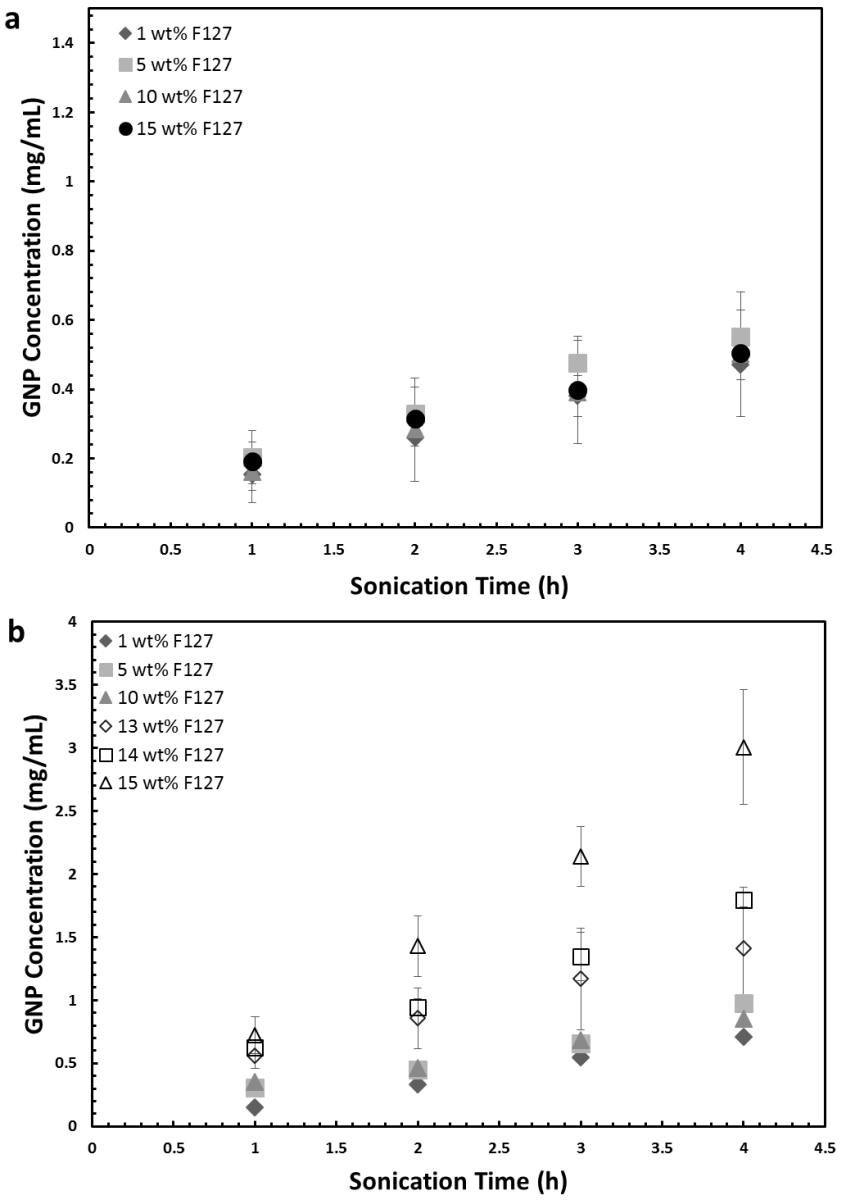

Figure 3.1: GNP concentration *vs*. time for various surfactant concentrations. (a) 70% amplitude. (b) 100% amplitude.

The effects of amplitude and amount of surfactant are further highlighted in Figure 3.2, which demonstrates that increasing the oscillation amplitude results in higher nanoplatelet concentrations. This figure also depicts the effect of surfactant concentration. At low and

medium sonication power, and above the Critical Micelle Concentration (CMC), the exfoliation yield appears to be independent of the amount of surfactant present in the system. However, the graphene concentration produced at high sonication power (100% amplitude) increases exponentially as the surfactant concentration increases beyond 10 wt%. The corresponding yield, with respect to the initial amount of graphite increases by an order of magnitude, from 0.6 to 6% at amplitudes of 35 and 100% respectively.

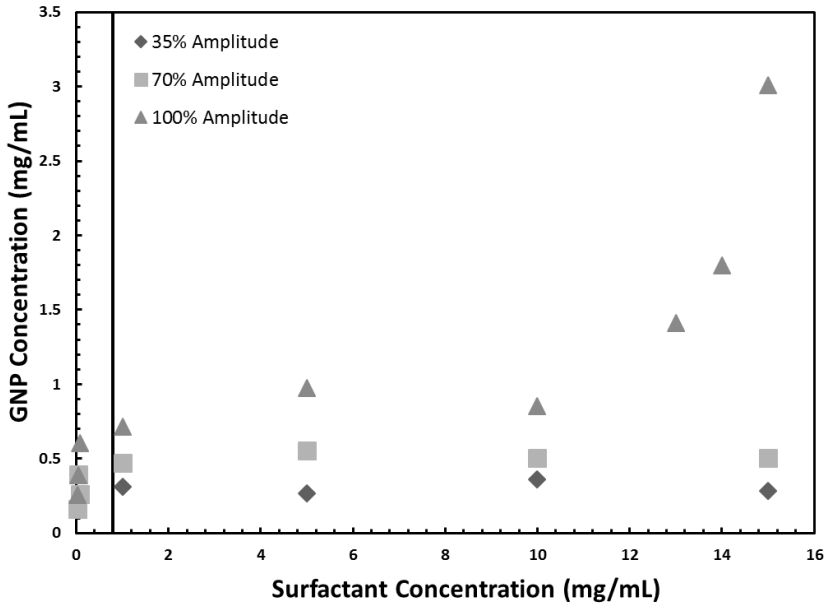

Figure 3.2: GNP concentration as a function of surfactant concentration, at three amplitudes (t=4 h). The vertical line indicates CMC at 20°C [110].

Dimensional analysis allows us to better understand the effect of power input, sample volume, and time on the graphene concentration produced by sonication. The performance of the system is described here in terms of five experimental parameters: initial graphite concentration (C_i), exfoliated graphite concentration (C), sonication time (t), power based on digital output on the sonicator (P), and solution volume (V). Figure 3.3 shows the experimental data in terms of the

dimensionless groups resulting from the Buckingham Π theorem (details are shown in Appendix B). The concentration (C) follows a power-law trend with respect to the dimensional group $P \cdot t^3 \cdot V^{-5/3}$, irrespective of the surfactant concentration, at surfactant concentrations below 10 wt% and constant initial graphite concentration, according to Equations (3.1)-(3.3):

$$35\%\ Amplitude: C = 5.64 \times 10^{-5} \left(PtV^{-\frac{5}{3}}\right)^{0.240} \tag{3.1}$$

$$70\%\ Amplitude: C = 5.53 \times 10^{-5} \left(PtV^{-\frac{5}{3}}\right)^{0.252} \tag{3.2}$$

$$100\%\ Amplitude: C = 2.26 \times 10^{-5} \left(PtV^{-\frac{5}{3}}\right)^{0.289} \tag{3.3}$$

The threshold where surfactant concentration becomes a variable in the production of GNPs is clearly visible in Figure 3.3. Specifically, above 10 wt% surfactant and at 100% amplitude, the concentrations of GNPs do not follow the trend lines described above, consistent with the experimental results described on Figure 3.1 and Figure 3.2.

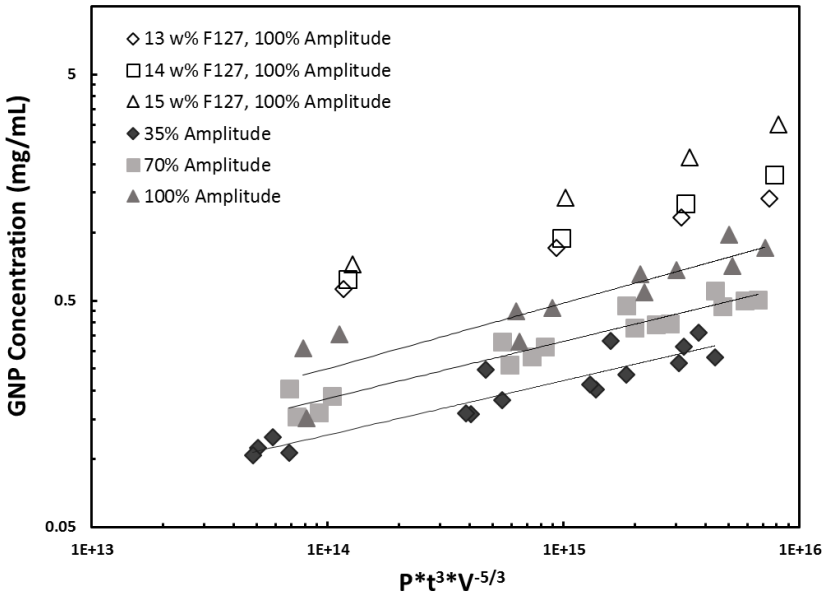

Figure 3.3: Dimensional groups showing the effect of power, time, and volume on graphene concentration. The trend lines represent the best fit for the data at each amplitude (summarized in equations (3.1)-(3.3). The open data points represent concentrations obtained at surfactant concentrations between 13-15 wt%.

3.3.2 Effects of sonication time, power and surfactant concentration on platelet size

The size of the GNPs being produced over the course of the exfoliation was studied with DLS. Figure 3.4 shows the influence of power and time on the mean nanoplatelet size at 5 wt% F127 in water. Similar trends were observed for the other surfactant concentrations. As the amplitude increases from 35% to 100% the particle size remains in the range of 200 to 300 nm. Furthermore, according to the DLS results, no discernible trend can be observed in the mean particle size variation over exfoliation time.

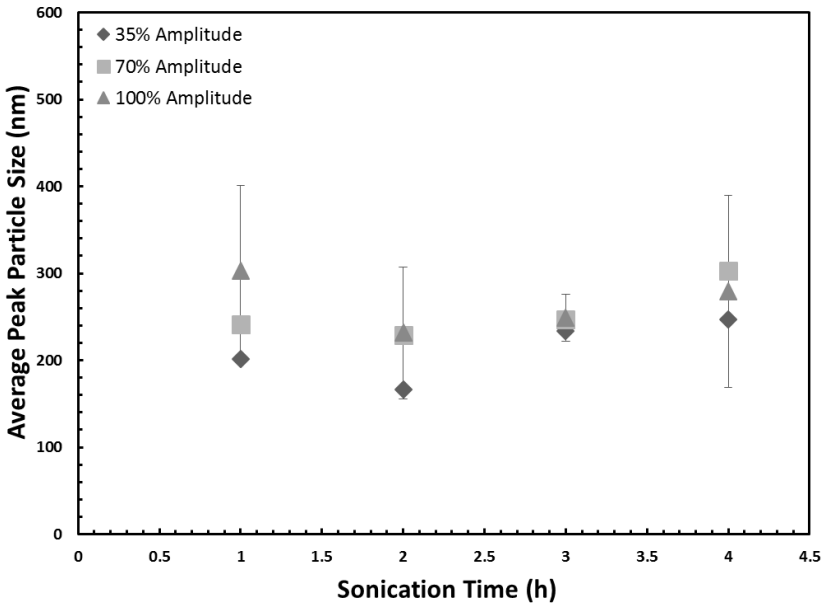

Figure 3.4: Effect of amplitude on the average particle size, obtained from three replicates of dynamic light scattering measurements at 5 wt% F127 in water.

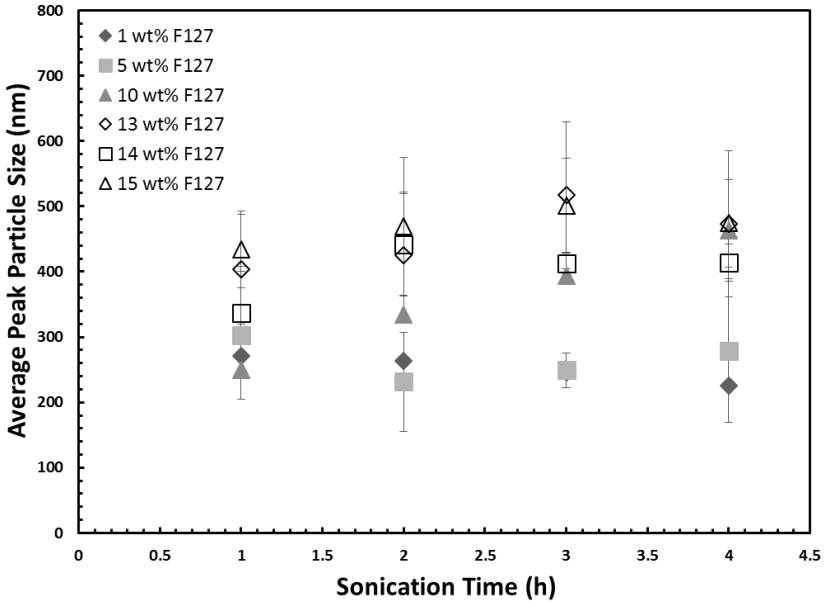

Figure 3.5: Effects of surfactant concentration on the average particle size obtained from three replicates, at 100% amplitude.

However, the average particle size increases, and the distribution becomes narrower when the surfactant concentration increases beyond 10 wt%, as shown in Figure 3.5 and Table 3.1.

Table 3.1: Effect of surfactant concentration on the average particle size (t=4 h) and polydispersity index (PdI) at 100% amplitude.

Surfactant Concentration (wt%)	Average Particle Size (nm)	PdI
1	251	0.261
5	266	0.174
10	360	0.326
13	455	0.031
14	401	0.033
15	470	0.031

.

3.3.3 GNP microstructure

Figure 3.6 shows representative TEM images of platelets produced at 100% amplitude at 1, 5, 14, and 15 wt% F127 in water. The contrast of the objects relates to their thickness: low-contrast images represent few-layer graphene (FLG) (Figure 3.7a, Figure 3.7b, and Figure 3.7e), whereas high-contrast images indicate multilayer graphene (MLG) (Figure 3.7d, Figure 3.7g, and Figure 3.7h). Overall, TEM data suggest that a wide range of nanoparticle thickness is being produced at all surfactant concentrations; however, it was observed that the occurrence of FLG nanoplatelets are more prominent at lower surfactant concentrations.

Image analysis on the TEM images support the DLS observations. At 1 and 5 wt% F127 in water, particle sizes range from about 200 to 400 nm, which is consistent with the DLS measurements (Table 3.1). At higher concentrations, the nanoplatelets are typically larger in size and multilayered.

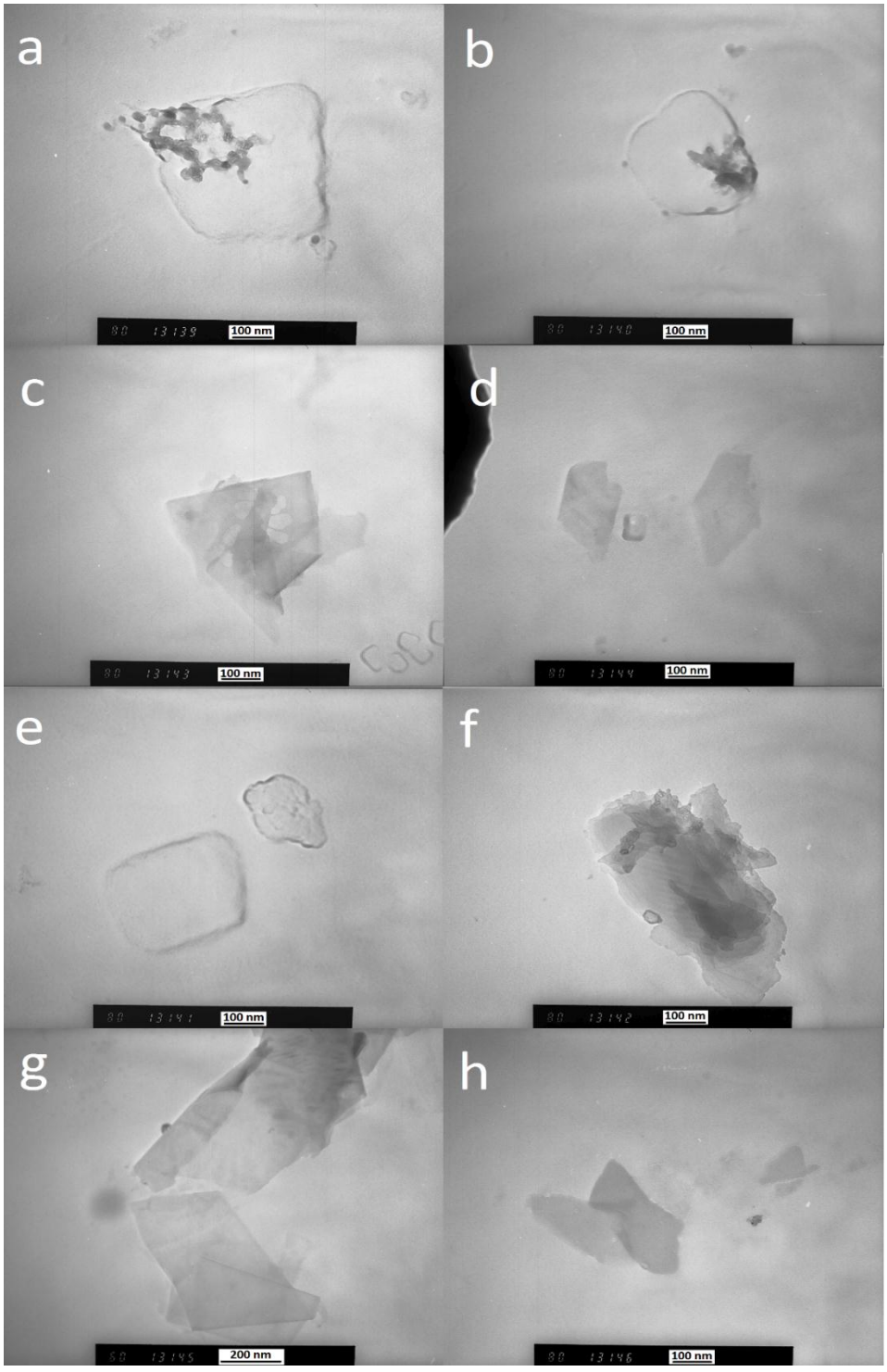

Figure 3.6: TEM images of GNPs produced at 100% amplitude and various surfactant concentrations (t=4 h). (a)-(b) 1 wt% surfactant concentration. (c)-(d) 5 wt% surfactant

concentration. (e)-(f) 14 wt% surfactant concentration. (g)-(h) 15 wt% surfactant concentration. Scale bar is 100 nm everywhere, except 7g (200 nm).

Since TEM imaging can only provide 2D information, AFM observations were used to complement the TEM images, and estimate the nanoplatelet thickness and thus obtain more information on the 3D dimensions of the graphene flakes produced during sonication. Figure 3.7a and Figure 3.7b display characteristic imaging of graphene sheets exfoliated at a surfactant concentration of 1 wt%, having a broad size distribution, ranging from from 70 to 350 nm. The platelet thickness distribution ranges from 4 to 5 nm, which is approximately equal to 6-9 stacked graphene layers The number of graphene layers is based on a single atom layer thickness of 3.4 Å [41] [50] [45] [111] (theoretical) and layer spacing of 3.35 Å [33] [35] [112]. Figure 3.7c and Figure 3.7d provide information on the size and thickness of the exfoliated material at a surfactant concentration of 15 wt%. A much broader distribution of size and thickness can be observed in this case. The lateral size (based TEM as they are considered more representative), thickness, stacked layers of graphene, and aspect ratio of the graphene platelets is summarized in Table 3.2. As in the case of TEM, it was consistently observed that, for both surfactant concentrations, flakes that were larger in size were also thicker.

Table 3.2: Summary of nanoplatelet properties using TEM and AFM measurements (100% amplitude and t=4 h).

Surfactant Concentration	Lateral Size, nm (TEM)	Thickness, nm (AFM)	Number of Stacked Graphene Layers	Aspect Ratio
1 wt%	324 - 431	4 - 5	6 – 9	72 - 108
15 wt%	294 – 540	8-77	13 - >100	7 - 65

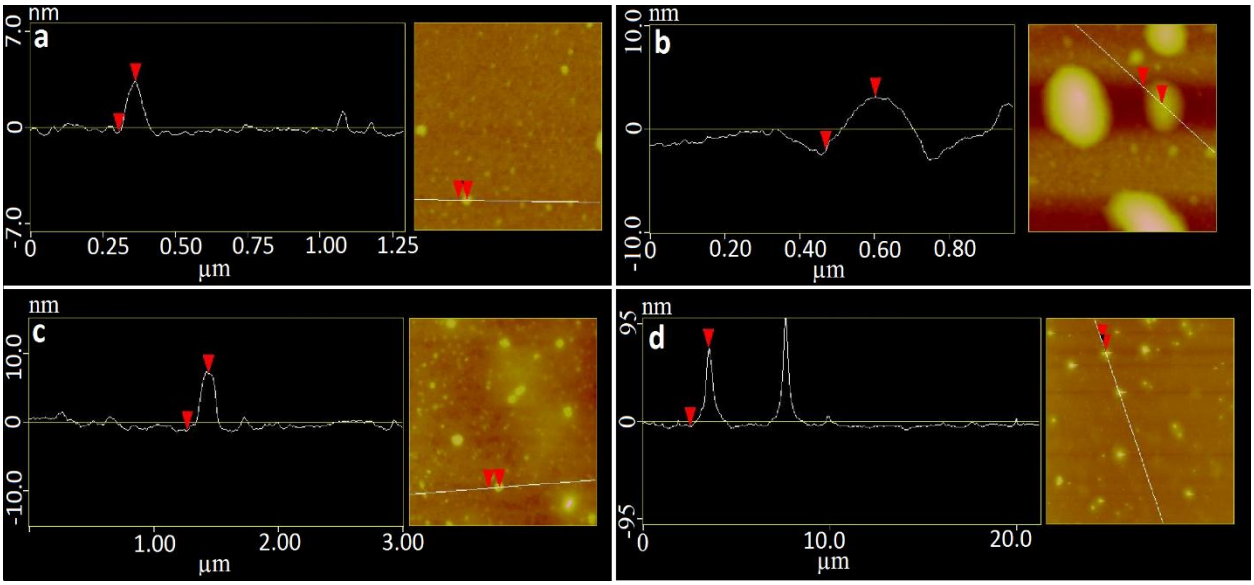

Figure 3.7: AFM images of GNPs at a surfactant concentration of 1 wt% and 15 wt% at 100% amplitude (t=4 h). (a)-(b) 1 wt% surfactant concentration. (c)-(d) 15 wt% surfactant concentration.

3.3.4 Specific surface area of GNPs

Figure 3.8 demonstrates the effects of surfactant concentration on the specific surface area (SSA) of graphene platelets, as measured by BET. Theoretically, it has been reported that graphene monolayers should have a specific surface area of 2630 $m^2 \cdot g^{-1}$ [113] while the surface area of few-layer graphene samples ranges from 280-1550 $m^2 \cdot g^{-1}$ [114]. Compared to literature, the specific surface area produced during exfoliation is lower and around 100 $m^2 \cdot g^{-1}$. The smaller particle size and higher aspect ratio at 1 wt% surfactant (Table 3.2) may account for the higher SSA recorded at this concentration.

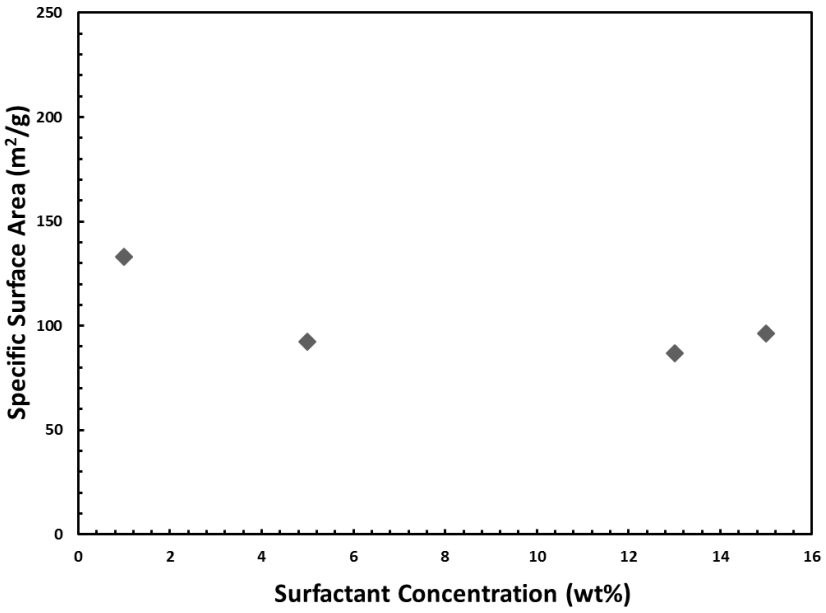

Figure 3.8: BET measurements on exfoliated GNPs produced at 100% amplitude at various surfactant concentrations.

3.4 Discussion

The experimental results presented above allow us to better understand the effects of sonication power and non-ionic surfactant concentration on the mechanism of graphite exfoliation in aqueous media. As summarized in Table 3.3, higher ultrasonic power densities are beneficial to the exfoliation yield and the production of GNPs correlates almost linearly within the range of power inputs examined (160-420 $W \cdot L^{-1}$). On the other hand, power changes did not have an effect on the mean platelet size, as assessed with DLS.

Surfactant concentrations below CMC (app. 1 wt%) result in less exfoliated material than concentrations above CMC (Figure 3.2). This observation can be explained by considering that micelles in the solution can serve as reservoirs of free surfactant that can replenish molecules adsorbed on the surface of the platelets during exfoliation. Above CMC the amount of surfactant had negligible effect on the exfoliation yield, and GNP size, within the concentration range 1-10

wt%. However, surfactant concentrations higher than 10 wt% at maximum power density (100% oscillation amplitude) improved the exfoliation yield by 3-fold or more, and resulted in increased GNP mean size by about 50%.

Overall the detailed parametric study and modeling based on dimensional analysis of this system has revealed that the threshold above which the concentration of the GNPs increases dramatically is between 70 and 100% amplitude and at or above 10 wt% surfactant. At these conditions, it is evident that a change in exfoliation mechanism takes place, resulting in higher yields of MLG, having aspect ratios of 7-65. Conversely smaller yields of FLG with aspect ratios about 72-108 are obtained at more moderate power inputs, and lower surfactant concentrations. Below we attempt to provide an explanation for these observations by examining the exfoliation mechanisms and the role of surfactant during the exfoliation process.

Table 3.3: Influence of experimental parameters on the exfoliation performance characteristics.

Experimental parameter	Graphene concentration	Platelet size	Aspect ratio
Sonication time	↑	unaffected	**(no data)**
Power input	↑	unaffected	**(no data)**
Surfactant concentration	unaffected (≤ 10 wt%) ↑ (> 10 wt%)	unaffected (< 10 wt%) ↑ (≥ 10 wt%)	↓

3.4.1 Graphite exfoliation mechanism – Effect of power input

In literature, the liquid phase exfoliation of graphite is usually assumed to be the result of layer by layer extraction of graphene from graphite, a mechanism called “delamination” [73] [115].

Gould et al. [116] identified three types of division in layered bulk systems: “stretching”, which represents equal separation of all layers, “cleavage”, which involves division into two sub-bulks, to form two new layered systems, and “*exfoliation*”, which stands for the removal of one layer from the top of a bulk (Figure 3.9). In our liquid exfoliation system, stretching is rather improbable, as it would require very long diffusion times for the liquid medium molecules to penetrate within the layers of the graphite and achieve separation of all layers.

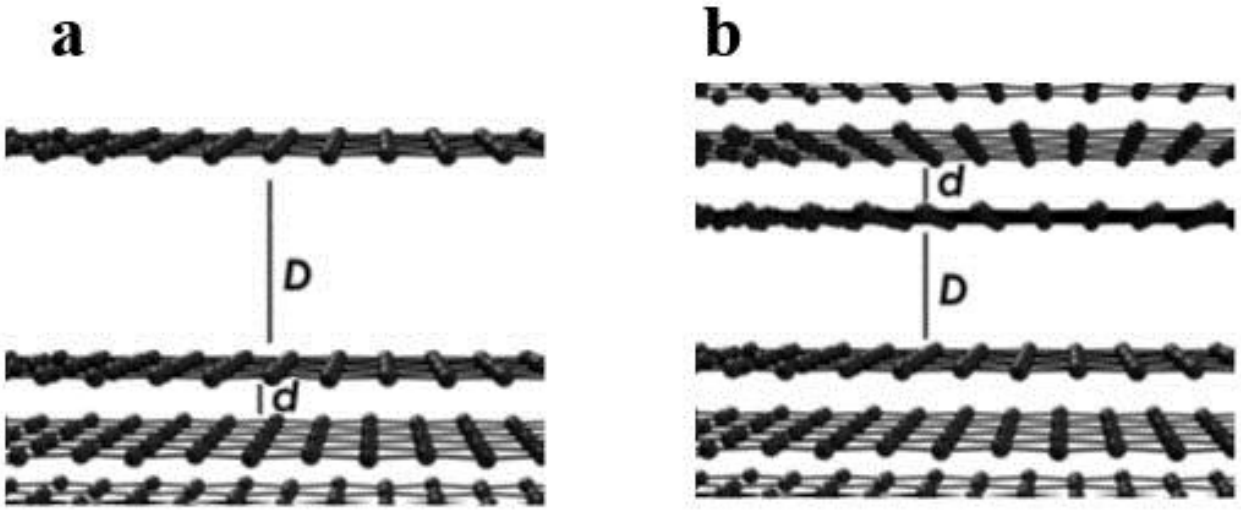

Figure 3.9: Graphene layers after (a) *exfoliation* and (b) cleavage [116]

Theoretical calculations performed by Gould et al. [116] show that *exfoliation* is a less energy-intensive process than cleavage. Specifically, the energy of interaction between the surfaces that are being separated varies with the inverse second power of separation (D^{-2}) in the case of cleavage and with $\log(D)D^{-3}$ in the case of *exfoliation*. Therefore, *exfoliation*, which involves separation of a single (or few layers) from the layered bulk appears to be prominent at the lower power densities and low surfactant concentrations, where low concentrations of FLG were obtained experimentally. As the power input to the system increases, the cleavage mechanism, which is a more energy-intensive process is promoted. Due to the nature of the mechanism, the

resulting GNPs will be multilayered and possibly larger in overall size. This conceptualization appears to explain our findings that at the highest power input, higher yields of multi-layered graphene particles are produced, whereas few-layer GNPs are more pronounced at the lower and medium power settings. Our results suggest that a threshold of power input must be reached before the cleavage mechanism begins to contribute significantly to GNP production.

3.4.2 Surfactant Concentration Effects on Graphene Concentration

In addition to the existence of a power input threshold, the concentration of surfactant plays a very important role. At maximum power density (100% oscillation amplitude) and surfactant concentrations higher than 10 wt% improvements in concentration and increases in the average particle size of the GNPs are observed. To the best of our knowledge, such a phenomenon has not been reported previously in the literature, possibly because graphite exfoliation by sonication is usually performed at surfactant concentrations around the CMC [19] [25]. In the sections below we interpret the effects of surfactant based on power/viscosity effects, as well as stabilization phenomena.

3.4.2.1 Effect of surfactant on the viscosity of the exfoliated medium

It is well known that increasing the surfactant concentration has a significant effect on the viscosity of the liquid medium. At the temperature of the experiments (20 ^{o}C), Pluronic F127 reaches a gel point around 17 wt% in water. Consequently, surfactant concentrations approaching gelation exhibit an exponential increase in viscosity. This effect is presented in Figure 3.10, which is a compilation of data from the literature [117] [118] [119] [120] and demonstrates that the viscosity of the aqueous phase varies exponentially in the concentration interval 1-15 wt%. The effect of surfactant concentration on viscosity is especially strong at 10

wt% or higher concentrations. It is, therefore, plausible that the increase in viscosity may have an effect on the exfoliation mechanism, by mediating more efficient transfer of shear forces from the medium to the graphite particles, thereby further promoting cleavage.

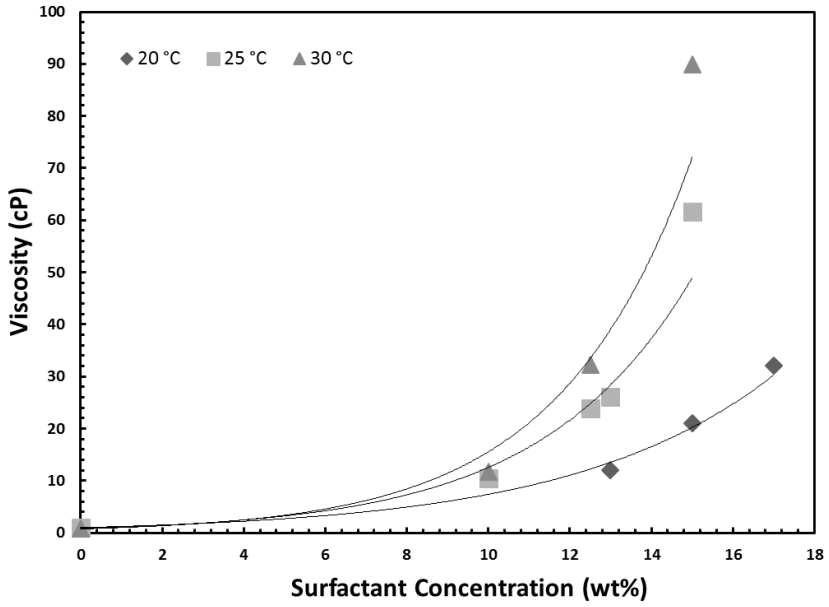

Figure 3.10: Viscosity of water-surfactant solution at various surfactant concentrations [117] [118] [119] [120].

The hypothesis that viscosity changes can correlate with exfoliation performance is examined below. Specifically, the data obtained at 100% sonication amplitude at different surfactant concentrations and times (Figure 3.11) were replotted after performing a viscosity normalization step. It was found that when all data were normalized with respect to one viscosity value, data disparity did not improve. Interestingly, when only results obtained at surfactant concentrations higher than 5 wt% were normalized, the data began to merge into a single band. The most narrow band was observed at viscosities around 6.5 cP, a value that corresponds to a surfactant concentration of approximately 10 wt%. As seen in Figure 3.11, at that viscosity the concentration lines begin to overlap. It is therefore possible that a viscosity threshold of

approximately 10 wt% exists, above which viscosity related effects begin to contribute to the exfoliation process.

At this point it must be acknowledged that the effect of viscosity is non-linear and, likely, complex. As power dissipation becomes more intense at elevated viscosities, changes in temperature profiles inside the system may ensue, further complicating the viscosity effect. This should therefore be a topic of further detailed investigation.

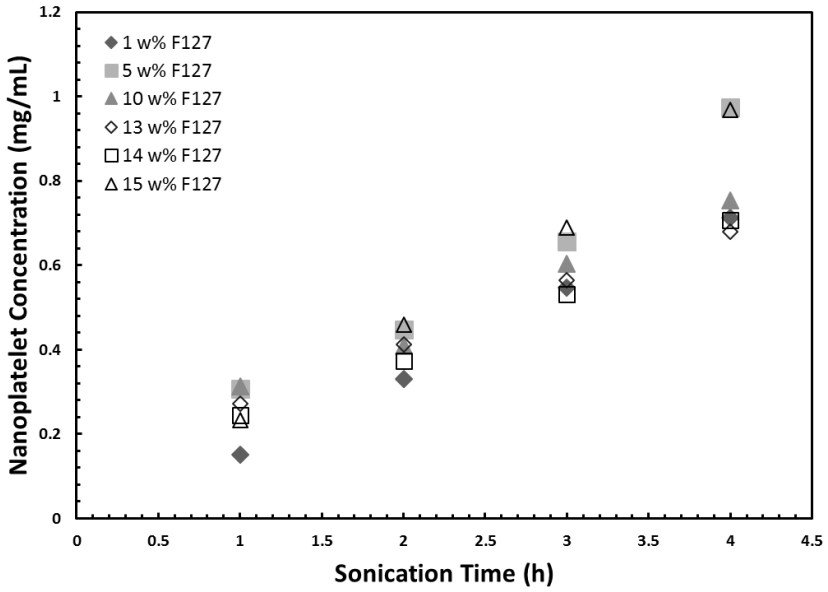

Figure 3.11: GNP concentration produced at maximum power density (100% oscillation amplitude) with a viscosity normalization.

3.4.2.2 Effect of surfactant on GNP stabilization

The effect of surfactant must also be considered in terms of its ability to stabilize the exfoliated GNPs. The amount of surfactant adsorbed on a GNP as a function of surfactant concentration was studied by means of TGA. As seen in Figure 3.12, the amount of surfactant that adsorbs on the nanoplatelets increases significantly with increasing surfactant concentration and sonication amplitude. Whereas the dependence is approximately linear at 70% amplitude, it becomes

exponential at 100% amplitude. Overall, the amount of surfactant retained with the GNP is significant, as it ranges between 0.08-0.28 g F127/g of dry nanoplatelets at 70% amplitude and between 0.22-0.56 g F127/g of dry nanoplatelets at 100% amplitude.

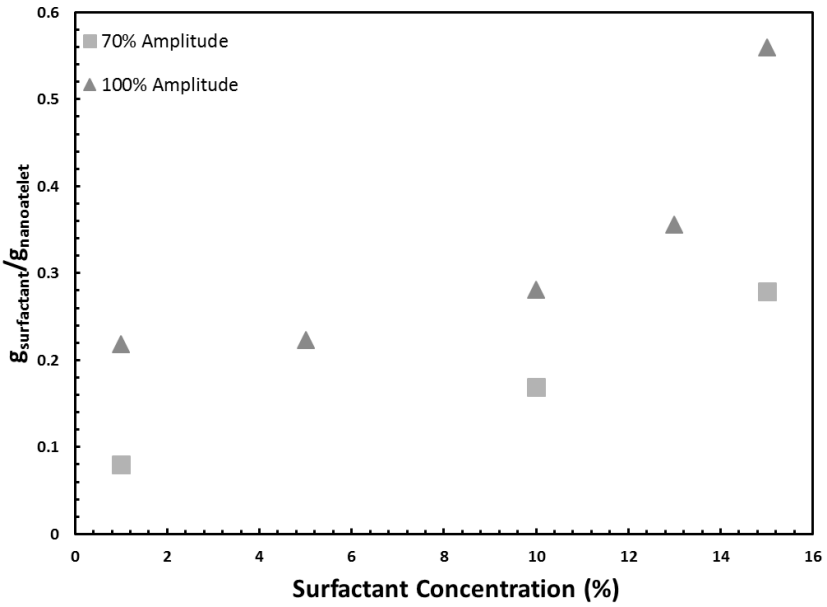

Figure 3.12: Thermogravimetric analysis on exfoliated GNPs, performed at various surfactant concentrations (t=4 h).

It has been shown that, at low concentrations (1 wt% or below), Pluronic F127 adsorbs on the surface of hydrophobic materials in the form of brushes of height approximately equal to 9 nm [121]. The adsorbed amount of F127 in a monolayer conformation has been calculated to be 0.543 mg m^{-2} on carbon black [122] and 1.8 mg m^{-2} on single-walled carbon nanotubes [123]. According to Figure 3.8 and Figure 3.12, the amount of adsorbed surfactant at 1 wt% F127 is of the order of 1.7 mg m^{-2} (0.22 g F127/g of GNP, $A_{sp}\approx130$ m^2/g), which supports the assumption that at this concentration the adsorbed F127 molecules form a monolayer on the surface of GNPs. At much higher concentrations, micelles are more likely to adsorb and cover the surface

of the GNPs rather than individual molecules [78] [124]. This assumption is also supported by our TGA and BET calculations, as follows. The micelles of F127 have been shown to have a radius of 9.2 nm and association number of 39 [122]. Assuming close packing of micelles at higher concentrations and a specific surface area of 90 $m^2 \cdot g^{-1}$ of GNP (Figure 3.8), a ratio of 0.28 g F127/g GNP is calculated. This value is very close to our TGA results for 10 wt% surfactant. TGA results also suggest that at concentrations higher than 10 wt% surfactant molecules adsorb much more densely on the GNP surface. The possibility that adsorbed surfactants assume higher-order configurations on GNPs at such high concentrations should not be discounted, although information on the packing of F127 molecules on the surface of graphene is currently not available in the literature. It is, therefore, possible that a fraction of larger particles formed at 100% amplitude and >10 wt% surfactant concentrations becomes stably suspended due to this higher density of adsorbed surfactants which cause stronger associations with the medium, and thus a higher resistance to sedimentation. This would increase significantly the concentration of GNPs that remain suspended in the supernatant and result in a larger mean particle size.

The observation that higher concentrations of surfactant cause an increased clustering of adsorbed micelles on the surface of GNPs may have multiple consequences. For example, part of the size difference between particles produced at lower vs. higher surfactant concentrations must be attributed to the adsorption of micelles, which are expected to increase the overall GNP size by a substantial amount. As mentioned earlier, a monolayer of adsorbed F127 molecules may have a thickness of approximately 9 nm, whereas the size of a micelle is close to 19 nm. Moreover, as the adsorption of micelles creates a higher density of hydrophilic groups on the surface of the nanoplatelets, hence a stronger association with the surrounding medium, the

diffusion rate of GNPs will be slower, thereby causing them to appear larger in a DLS measurement.

3.5 Conclusion

Poloxamer based surfactants have been shown to produce high concentrations of graphene through the ultrasonication exfoliation of graphite. The concentration is dependent on the amplitude (power) of the sonicating tip and length of exfoliation where larger amplitudes and longer exfoliation times increase the concentration of GNPs (0.26-3.01 $mg \cdot mL^{-1}$). At lower surfactant concentrations (≤10 wt%) average particle sizes were found to range from 250-360 nm. Increasing the surfactant concentration (>10 wt%) enables the stabilization of larger particles (~500 nm) due to micelle association and the formation of multilayer surfactant adsorption on the nanoplatelet surface. Coupling high amplitudes with high surfactant concentrations produces exponentially increased nanoplatelet concentrations. Thus, it is believed that both *exfoliation* and cleavage mechanisms are responsible for the exfoliation of graphite where cleavage becomes more prominent at maximum power. The quality of the nanoplatelets was affected by the surfactant concentration where larger surfactant concentrations produced thicker GNPs. Thus, the aspect ratios were estimated to range from 72-108 and 7-65 at surfactant concentrations of 1 wt% and 15 wt%, respectively. This work demonstrates that Pluronic® F127-assisted ultrasonication exfoliation water can produce high concentrations of stable GNP dispersions in an environmentally friendly manner.

Chapter 4: Exfoliation via Shear Mixing

4.1 Introduction

The production of large quantities of graphene is a sought-out process hindered by the low efficiencies of current methods. Bottom-up methods are excellent at creating pristine single layer graphene molecules. These methods, such as chemical vapour deposition, are highly controllable in terms of sheet size and thickness, making them great approaches for producing graphene usable within electronics. However, the production rates are typically very low, making them difficult to implement industrially [125] [126] [127]. In top-down methods, production rates can be higher but the wide range of sheet thicknesses produced limits their applications in electronics. Liquid phase exfoliation and covalent modification methods have shown promise for generating highly concentrated solutions of graphene [54] [60] [61] [62] but with long processing times. Liquid phase exfoliation typically uses ultrasonication as the exfoliation source which requires 24 h [61] to 400 h [54] [60] depending on the liquid media to produce appreciable amounts of graphene.

However, ultrasonication is not scalable because of the large amounts of energy that would be required from industrial sized instruments. Recently, application of high shear forces through the use of shear mixers [58] and microfluidization [59] have been investigated as scalable methods of graphite exfoliation. The production rates for each method are exceptional, reaching as high as 1.44 $g \cdot h^{-1}$ and 9.3 $g \cdot h^{-1}$, respectively, with larger production rates upon scale-up. Shear exfoliation is similar to liquid phase exfoliation as aqueous liquids can be used to facilitate the exfoliation of graphite and provide a stable dispersion of graphene thereby eliminating the use of harmful organic liquids. However, research in aqueous systems using non-ionic surfactants is

limited as ionic surfactants [58] [59] and organic solvents [58] [128] have been the main focus for exfoliating agents. As previously stated, liquid phase exfoliation in non-ionic surfactant systems performed better than ionic surfactants providing better stability and higher concentrations of graphene nanoplatelets [61] [62] [73] [77]. Furthermore, characterization of the graphene nanoplatelets produced in different exfoliation conditions is limited in the literature.

Herein, a detailed study is conducted on the effect of a wide-range of operating conditions and concentrations of a non-ionic surfactant system on the yield and properties of the resulting graphene nanoplatelets produced by shear mixing. The acquired data prove that this method of exfoliation can produce high concentrations of good quality graphene nanoplatelets with the potential for easy scalability.

4.2 Experimental Section

4.1.1 Materials

Natural graphite powder (purity 95%) was supplied by Eagle Graphite and purified (99%) with anhydrous ethyl alcohol and acetone. Pluronic® F127 was purchased from Sigma Aldrich and used as received. Milli-Q quality water was used in all of the experiments.

4.1.2 Methods

Graphite (G) was exfoliated using a Silverson L5M-A shear mixer equipped with a 3 cm diameter square hole stator. Various surfactant concentrations were used for the exfoliation process and prepared by dissolving Pluronic® F127 in Milli-Q water to a total volume of 180 mL. Since the dissolution of Pluronic® F127 in water is more favourable at lower temperatures, the mixture was left to equilibrate for 12 h at 4 °C. Graphite powder (5 wt%) was added to the

surfactant solution and stirred until adequately mixed. The graphite-surfactant solution was placed in a temperature controlled bath to maintain temperature at approximately 20 °C (room temperature). Graphite exfoliation was initiated after lowering the rotor three quarters down (off centered) into the solution volume and setting the rotation speed. The solution was left to exfoliate for 1 hour with samples taken in 10 minute intervals. These samples were centrifuged at 1800 g for 30 minutes and the supernatant was used for characterization through UV-VIS spectroscopy and DLS.

4.1.3 Instrumentation and Analysis

UV-VIS spectroscopy was performed on a Varian Cary 100 Scan spectrophotometer. The selected wavelength range was from 400 to 800 nm and the cuvette path length was 0.01 m. The absorbance was converted to concentration using the Lambert-Beer law. The supernatants of the centrifuged samples were diluted 10-20 fold with Milli-Q water to ensure the absorbance was within the instrument's range.

The extinction coefficient used in these experiments was analytically determined using the Lambert-Beer law with two different methods (Appendix C). First, the absorbance of a known volume was measured using UV-Vis and sequentially dried using a vacuum oven. After drying, the adhered surfactant was removed in an inert atmosphere using TGA and the mass of the dry material was measured. Thus, the concentration of graphene nanoplatelets was determined by dividing the mass of the dry material by the sample volume. Plotting the absorbance against the nanoplatelet concentration provided the extinction coefficient as the slope of the trend line. In the second method, a known mass of dry, surfactant free material was dispersed in a known volume of NMP. After, the absorbance of the solution was measured using UV-Vis and then plotted

against the concentration similar to the previous method. Both methods were in agreement and were averaged to produce an extinction coefficient of 732 $mL \cdot mg^{-1} \cdot m^{-1}$ (λ=660 nm) (Figure C.1 and Figure C.2). This is lower than results reported in literature [54] [104] [105] [106], though the extinction coefficient appears to be dependent on the system in which the nanoplatelets were exfoliated [107].

The samples were further diluted (15-fold) with Milli-Q water and estimates of the particle size distribution of the graphene nanoplatelets were obtained through Dynamic Light Scattering (DLS) measurements, using a Malvern Instruments Zetasizer Nano ZS (λ=633 nm). The polydispersity index (PdI) in DLS measurements describes the width of a particle size distribution and is calculated from a Cumulant analysis [108]. Thus, true monodisperse solutions inherently have PdI values of 0. However, the classification of monodisperse ranges from 0.0-0.1 whereas polydisperse ranges from 0.1-0.7 [109]. Values > 0.7 indicate samples that are not suitable for DLS [108]. Data obtained through DLS, however, must be interpreted with caution as the reported particle size, calculated from the Stokes-Einstein equation, is that of the spherical equivalent of GNP. Furthermore, the DLS intensity averages are affected more by larger particles than smaller particles. Thus, it must be taken into account that the larger particles will have a greater affect on the particle size distribution when interpreting the PdI.

Prior to thermogravimetric analysis (TGA), the solutions were filtered through a 0.2 □m pore size Sterlitech Nylon membrane filter and washed to remove any excess surfactant. The powder was collected and sequentially dried in a vacuum oven at 60 °C for 12h. Thermogravimetric analysis was carried out using a Q500 TGA instrument from TA instruments. Samples were heated from room temperature to 400 °C at 20 $°C \cdot min^{-1}$ under a 50 $mL \cdot min^{-1}$ nitrogen gas flow.

Isothermal conditions were maintained at 400 °C for 45 minutes before ramping up to 450 °C at 20 °C·min^{-1} to ensure all of the surfactant was degraded.

BET measurements were conducted using an Autosorb-1 by Quantachrome instruments to obtain the specific surface area of the graphene platelets. Samples obtained from TGA were degassed at 300 °C for 4 h and then analyzed using multipoint BET physisorption with nitrogen relative pressures (0.1-0.3 at 77 K).

TEM images were obtained using a Hitachi H-7000 instrument operated at 75 kV. Dry graphene powder was first dispersed in NMP at 0.1 wt% using an ultrasonic bath for 1.5 h. The sample was then deposited on 300 mesh copper grids and dried before analysis.

The graphene nanoplatelet-NMP solution was spray coated onto a silicon wafer in preparation for atomic force microscopy (AFM) measurements. To prevent ring effects from occurring, the silicon wafers were spray coated while laying on a hot plate to increase the evaporation rate of NMP. Measurements of graphene platelet thickness were carried out using a Veeco Di NanoScope llla AFM, with an AppNano ACT N-type silicon probe (force constant k=37 N·m^{-1}, radius of curvature=6 nm, resonance frequency f=300 kHz) in tapping mode.

4.4 Results

4.2.1 Effect of Surfactant Concentration on Graphene Nanoplatelet Concentration and Size

Consistent with the results presented in Chapter 3, a linear relationship exists between the graphene concentration and exfoliation time. Shear exfoliations were conducted at different surfactant concentrations to determine the effect of surfactant concentration on the concentration

of graphene. Due to excessive frothing, the system was unable to be operated at 15 wt% F127. Thus, only surfactant concentrations at 1, 5, and 10 wt% were investigated. Overall, the three surfactant concentrations showed similar trends with respect to time.

Increasing the surfactant concentration from 1 wt% to 10 wt% resulted in slightly lower graphene nanoplatelet concentrations. After 1 hour of exfoliation, the graphene concentration was 0.055 $mg \cdot mL^{-1}$, 0.046 $mg \cdot mL^{-1}$, and 0.036 $mg \cdot mL^{-1}$ at 1 wt%, 5 wt%, and 10 wt% F127 in water, respectively (Figure 4.1). Equivalently, the yields, with respect to the initial graphite concentration, after 1 hour of mixing were 0.20 %, 0.17 %, and 0.13 % at 1 wt%, 5 wt%, and 10 wt%, respectively.

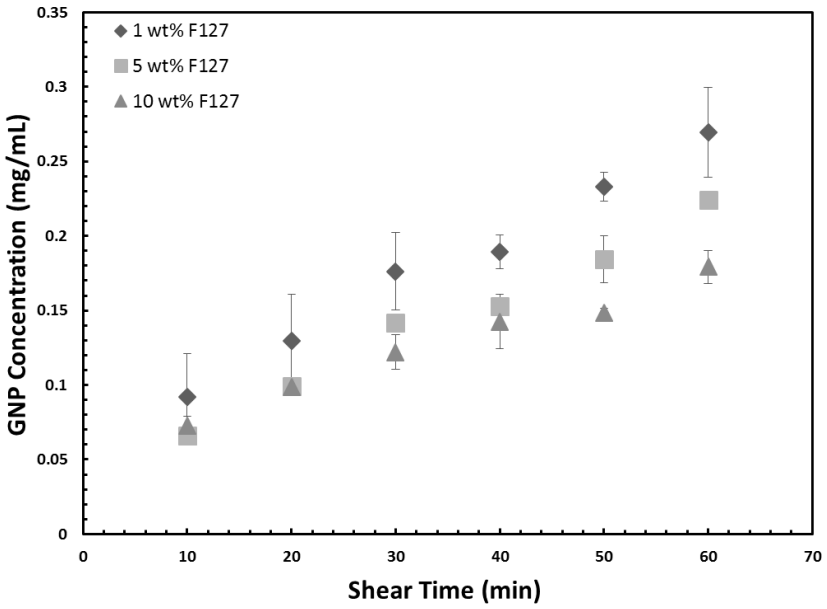

Figure 4.1: Effect of surfactant concentration on the graphene nanoplatelet concentration in a shear exfoliation process at 6000 rpm.

Overall the surfactant concentration did not affect substantially the graphene nanoplatelet concentration in the shear exfoliated system. However, it should be noted that in the batch

sonication system the important differences were seen at surfactant concentrations above 10 wt%, which were not tested in the present case.

Figure 4.2 shows the average particle size as a function of sampling time at surfactant concentrations of 1 wt%, 5 wt%, and 10 wt%. Particle size increased from ~250 nm at 1 wt% surfactant solution to ~450 nm at 10 wt% surfactant solution. Table 4.1 displays the particle size distribution for the conditions in Figure 4.2. Appendix F visually displays the particle size distributions (Figure F.1, Figure F.2, and Figure F.3). However, the particle size was not affected by the surfactant concentration at lower surfactant concentrations, as there is a negligible difference between 1 wt% and 5 wt%. On the other hand, increasing the surfactant concentration up to 10 wt% results in roughly double the particle size. Such phenomenon was also witnessed in batch sonication systems, where a threshold existed beyond which the particle size began to increase with increasing surfactant concentration, as explained in Chapter 3 and is likely the result of larger particles remaining in suspension in the presence of higher amounts of surfactant.

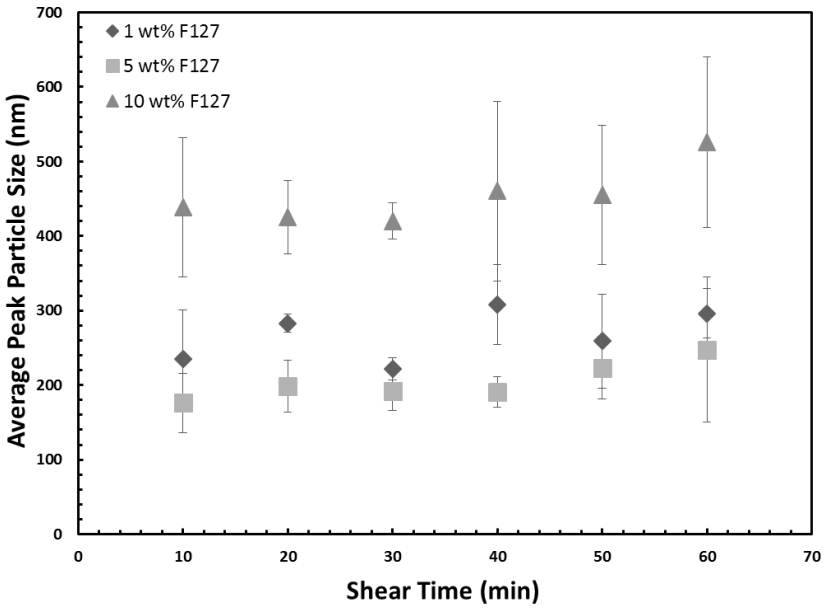

Figure 4.2: Mean particle size determined from three separate measurements for each individual surfactant concentration. Surfactant concentrations were examined at 1 wt%, 5 wt%, and 10 wt% at 6000 rpm.

Table 4.1: Average particle size and polydispersity index for various surfactant concentrations conditions exfoliated at 6000 rpm and t=1 h.

Surfactant Concentration (wt%)	Average Particle Size (nm)	PdI
1	267	0.253
5	205	0.140
10	454	0.271

This hypothesis is supported by the TGA analysis, which shows that the amount of adsorbed surfactant on the surface of the platelets increases with initial surfactant concentration (Figure 4.3)

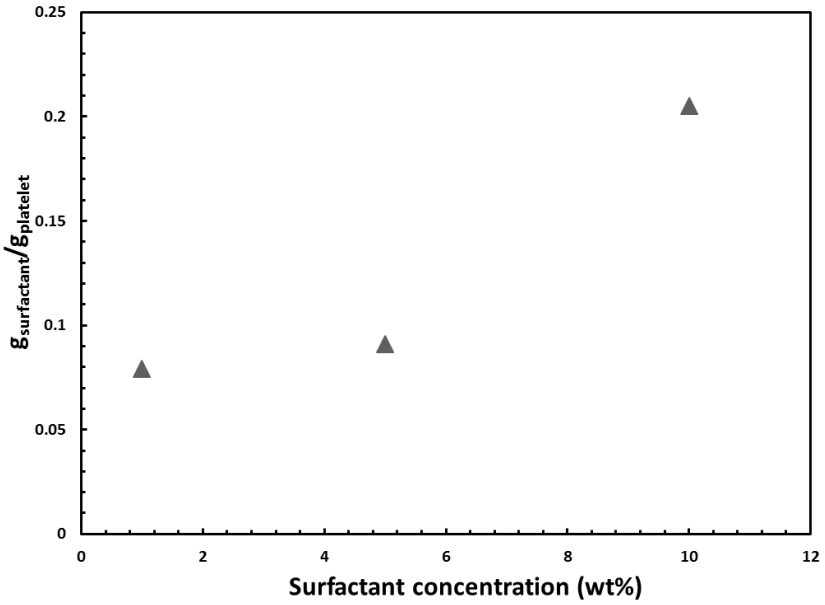

Figure 4.3: Thermogravimetric analysis on graphene nanoplatelets showing the amount of adsorbed surfactant as a function of initial surfactant concentration (t=1 h).

Adsorption of poloxamer is a phenomenon affected by the concentration. As the concentration of surfactant in solution approaches CMC, more of the surface of a hydrophobic material is covered by the polymer. In addition, as micelles form they begin to associate with themselves leading to a higher packing order on the hydrophobic surface. Therefore, an increase in the amount of surfactant adsorbed on the graphene platelets as the bulk concentration of surfactant increases is to be expected.

4.2.2 Effects of Rotor Speed on the Graphene Nanoplatelet Concentration

It is known that the concentration of exfoliated graphite is dependent upon the shear forces applied to graphite particles, which in turn are generated by the spinning of the rotor. Thus, it is expected that controlling the rotation speed of the rotor will also control the amount of graphite that is exfoliated. Figure 4.4 confirms that as the rpm of the shear mixer is increased the

concentration of exfoliated graphite increases as well. For these experiments, surfactant concentrations of 1 wt% were used due to a slightly better performance over other concentrations (Figure 4.1). After 1 hour of exfoliation, the concentration of exfoliated graphite was 0.05 $mg \cdot mL^{-1}$, 0.24 $mg \cdot mL^{-1}$, 0.27 $mg \cdot mL^{-1}$, and 0.36 $mg \cdot mL^{-1}$ at rotation speeds of 1500, 4500, 6000, and 8000 rpm, respectively. Equivalently, the yields, with respect to the initial graphite concentration, were 0.096 %, 0.48 %, 0.54 %, and 0.72 % at rotation speeds of 1500, 4500, 6000, and 8000 rpm, respectively.

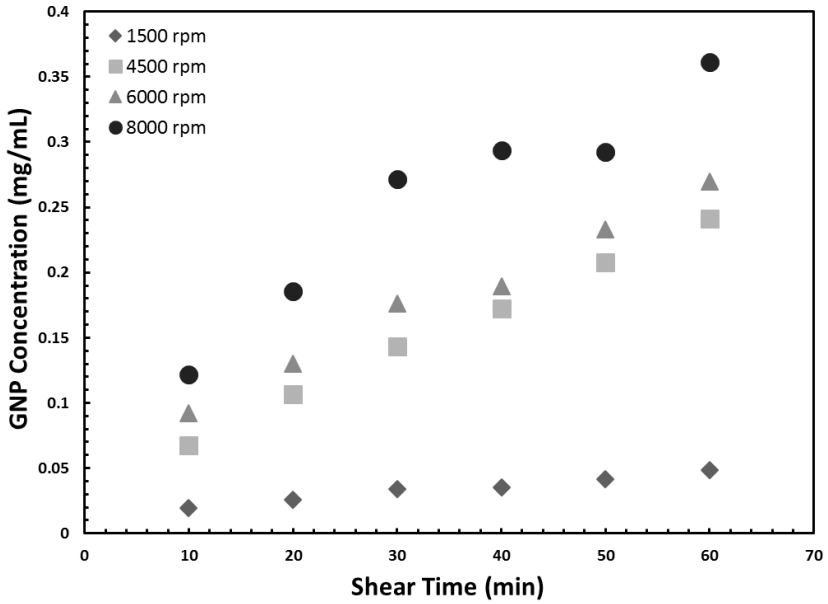

Figure 4.4: Graphene concentration as a function of shearing time at various rotor speeds in a 1 wt% surfactant solution. The concentration is dependent on the rpm of the rotor.

To understand the relationship between rotor speed and the resulting concentration of exfoliated graphite, a dimensional analysis was performed using the following six parameters: exfoliated graphite concentration (C), initial graphite concentration (C_i), rotor speed (N), shearing time (t), rotor diameter (D), and solution volume (V). However, in these experiments the initial graphite concentration, rotor diameter, and solution volume were kept constant. The experimental data are

plotted, using the resulting dimensional groups in Figure 4.5. This figure clearly shows that there is a difference in low rotor speeds (1500 rpm) and higher rotor speeds (≥4500 rpm). Data obtained at high rotor speeds lay on the master curve according to which the exfoliated graphite concentration depends upon the product of rotation speed and time according to equation 4.1.

$$C = 1.24 \times 10^{-5}(Nt)^{0.661} \tag{4.1}$$

While the concentration of exfoliated graphite is also proportional to time at the lowest rotor speed of 1500 rpm, the data do not match the master curve and are described by a different relationship. This difference demonstrates that the system is lacking in rotor speed to efficiently exfoliate the graphite particles, below a rotation speed threshold.

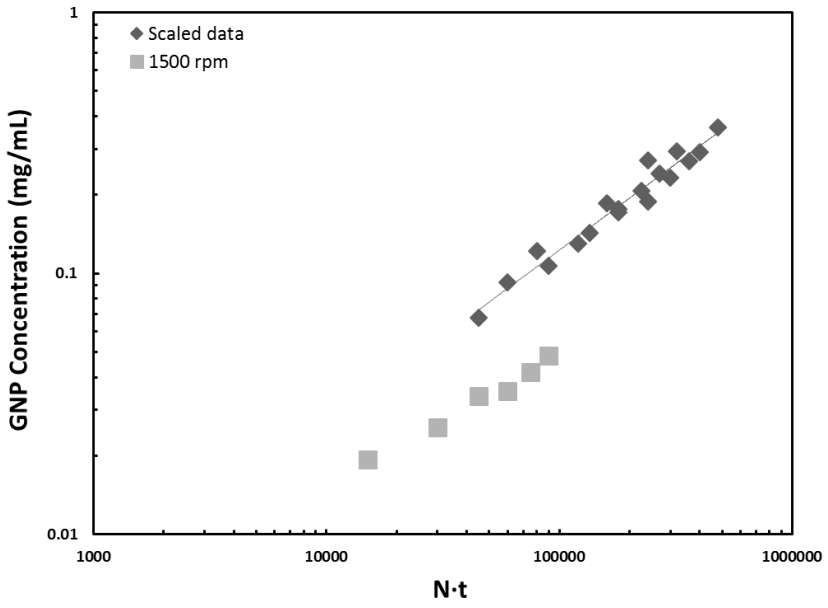

Figure 4.5: Dimensional analysis of the parameters involved in the exfoliation of graphite by shear mixing. The data are fitted according to a power-law scaling relation, shown in equation (4.1).

It is well known that graphite consists of individually stacked layers of graphene that are held together by van der Waals forces. For exfoliation to occur, the applied forces must overcome the van der Waals attraction forces through parallel motion (e.g. peeling - scotch tape method) or perpendicular motion (e.g. shear exfoliation).

Since the shear force is directly relatable to the rotor speed, higher rotor speeds (i.e. higher shear forces) will produce more exfoliated graphite in a given time period. However, there exists a threshold in the shear force where the efficiency of the exfoliation process substantially increases. Paton *et al.* demonstrated that a minimum shear rate is required to produce high concentrations of exfoliated graphite in NMP [58]. Concentrations obtained after 1 minute of mixing were compared to various shear rates where the shear rate was determined by $\dot{\gamma} \approx \pi ND/\Delta R$ where ΔR is the rotor-stator gap. The data suggested that a minimum shear rate of 10^4 s^{-1} was required to exfoliate graphite. Thus, at conditions of 1500 rpm, diameter of 25 mm, and a rotor-stator gap of 5 mm, the exfoliation system conducted in this experiment is at a shear rate of approximately 5000 s^{-1}. The system can produce relatively small quantities of exfoliated graphite but the shear rate is not high enough to efficiently exfoliate the graphite particles. At conditions of $N \geq 4500$ rpm, the shear rates approach shear rates of 15000 s^{-1} where shear forces are much greater than the van der Waals forces. Increasing the rotor speed past 4500 rpm results in larger exfoliated graphite concentrations due to faster processing and throughput of material at the rotor. Hence, the separation of the data collected at 1500 rpm from the master curve is caused by insufficient shear rates thereby decreasing the production rate of exfoliated graphite.

4.2.3 Graphene Nanoplatelet Morphology

While DLS results described above offered insight on the average particle size, they operate under a spherical model assumption, and thus do not provide any information on the actual 3D dimensions and aspect ratio of the graphene nanoplatelets. TEM imaging offers a more exact representation of graphene nanoparticles and can be used to complement DLS measurements. The size, shape, and dimensions of graphene nanoplatelets produced from shear mixing at 6000 rpm was studied using TEM. Figure 4.6 demonstrates that the dimensions of the platelets produced at surfactant concentrations of 1 wt% and 5 wt% agrees with the DLS results. The particle sizes did not drastically vary between the two surfactant concentrations, and lateral measurements ranged from 240 to 440 nm; matching well with the peak averages from DLS.

The images agree with literature reports in terms of size and contrast [58] [129]. Low contrast indicates low thickness, which would be a result of layer by layer extraction of graphene nanoplatelets, representing monolayer to few-layer structures. This structure would be expected when layer-by-layer exfoliation takes place. Mixtures of few-layer graphene nanoplatelets (Figure 4.6a and Figure 4.6c) and multilayer graphene nanoplatelets are present; the latter are evident by the high contrast in Figure 4.6b and Figure 4.6d. In addition, folding [61] [73] occurs within nanoplatelets produced by shear mixing [58] [130] (Figure 4.6c and Figure 4.6d). However, folding was present in a high degree which is not uncommon, owing to the conditions encountered during shear mixing [58] [130].

Based on the images it appears that the surfactant concentration did not affect the quality of the graphene flakes as both few-layer and multilayer graphene nanoplatelets were generated at both surfactant concentrations. This is consistent with the DLS findings, which showed that increasing

the surfactant concentration from 1 wt% to 5 wt% did not have any effect on the size of the graphene nanoplatelets.

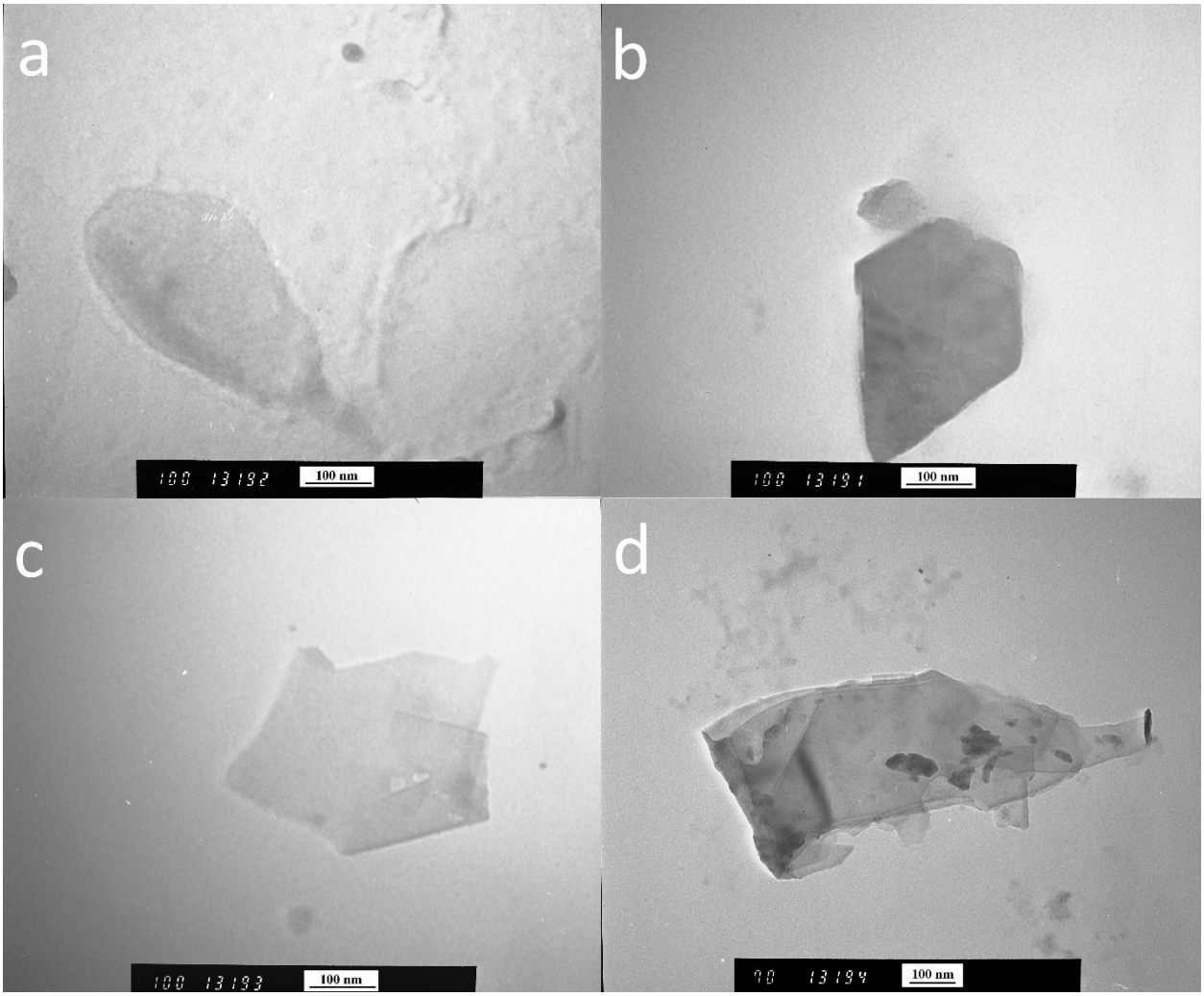

Figure 4.6: TEM images of graphene nanoplatelets produced at 6000 rpm at two different surfactant concentrations (t=1 h). (a)-(b) 1 wt% surfactant concentration. (c)-(d) 5 wt% surfactant concentration.

Estimation of the platelet thickness is not possible based on TEM. Atomic force microscopy (AFM) measurements were performed to determine the sheet thickness and obtain more information on the size distribution of graphene flakes produced during shear mixing. Between

the two surfactant concentrations, a range of sheet thickness and size was observed. Figure 4.7a is a measurement of graphene nanoplatelets exfoliated at a surfactant concentration of 1 wt%. From the image, the thickness was measured at 11 nm. Figure 4.7b demonstrates the nanoplatelet size and thickness of a flake exfoliated at a surfactant concentration of 5 wt%. The thickness of the nanoplatelet was measured to be 6 nm. The lateral size (based on TEM as they are considered more representative), thickness, stacked layers of graphene, and aspect ratio of the graphene platelets are summarized in Table 4.2.

Table 4.2: Summary of nanoplatelet properties using TEM and AFM measurements (rotation speed=6000 rpm and t=1 h).

Surfactant Concentration	Lateral Size, nm (TEM)	Thickness, nm (AFM)	Number of Stacked Graphene Layers	Aspect Ratio
1 wt%	230 - 440	11	17	21 - 40
5 wt%	299 – 555	6	10	50 - 92

The number of layers from each system were calculated based on a single atom layer thickness of 3.4 Å [41] [45] [50] [111] (theoretical) and layer spacing of 3.35 Å [33] [35] [112]. Similar to DLS results, surfactant concentrations of 1 wt% had on average larger particle sizes than at 5 wt% (based on Figure 4.7).

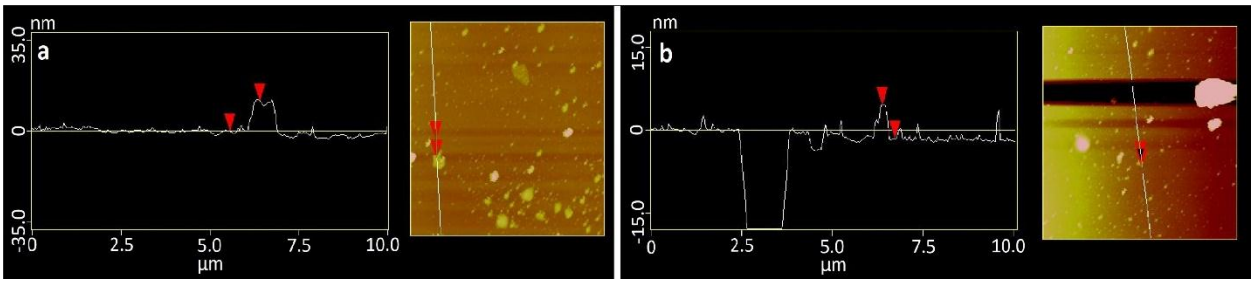

Figure 4.7: AFM images of graphene nanoplatelets at a surfactant concentration of 1 wt% and 5 wt% at 6000 rpm for 1 h. (a) 1 wt% surfactant concentration. (b) 5 wt% surfactant concentration.

Paton *et al.* demonstrated average thicknesses around 7-8 [58] layers in sodium cholate solutions while Karagiannidis *et al.* observed an average thickness of approximately 18 layers using microfluidization in sodium deoxycholate (SDC) [59]. In addition, Karagiannidis *et al.* showed that with more cycles through the microfluidizer the distribution of the platelet thickness shifted towards a lower thickness.

4.5 Conclusions

Shear mixing is a promising, scalable and industrially relevant method to produce high concentrations of graphene nanoplatelets. Shear exfoliation in Pluronic® F127 accomplished nanoplatelet concentrations comparable to ultrasonication and followed a simple scaling factor with rotor speed. Increasing the rotor speed increased the shear forces applied to the graphite particles resulting in a higher concentration of graphene nanoplatelets (0.05-0.36 $mg \cdot mL^{-1}$). The particle sizes of the nanoplatelets were slightly affected by the surfactant concentration, which enabled the stabilization of larger particles (200-450 nm). Regardless, the quality of the nanoplatelets was largely unaffected by the surfactant concentration and were found to be >10 layers in thickness, with estimated aspect ratios of 25 to 40 and 52 to 72 produced in surfactant concentrations of 1 wt% and 5 wt%, respectively. This work demonstrates that Pluronic® F127 -

assisted shear exfoliation in water can produce concentrations of GNPs that are similar to those reported in organic media, and therefore provides a more environmentally friendly alternative to organic solvents.

Chapter 5: Conclusions and Future Work

5.1 Conclusions

This work studied the characteristics of liquid-phase exfoliation of graphite in water with the aid of the non-ionic surfactant Pluronic® F127. Two types of exfoliation processes were examined: ultrasonication and shear mixing. The effect of surfactant was explored over a wide range of concentrations: below CMC (approximately 1 wt% at 20 ^{o}C) up to 15 wt% (close to the surfactant's gelation point at 20 ^{o}C). Ultrasonication results showed that the nanoplatelet concentration can be controlled through the amplitude (power) of the sonicating tip where higher amplitudes increase the nanoplatelet concentration up to 3 mg·mL^{-1}. On the other hand, shear mixing can control the nanoplatelet concentration through the rotor speed. Increasing the rotor speed increases the shear forces in the systems and enhances the exfoliation of graphite achieving GNP concentrations up to 0.36 mg·mL^{-1} after one hour of mixing. Using dimensional analysis, a master curve that relates the GNP concentration to the processing parameters was generated ($C \sim C_i \cdot V \cdot N \cdot t \cdot D^{-3}$) and demonstrated a rotor speed threshold above 1500 rpm. The scaled data indicates excellent potential for scalability and followed the general equation of $C = 1.24 \times 10^{-5}(Nt)^{0.661}$.

The concentration of the surfactant played a role in the production of graphene nanoplatelets. Lower surfactant concentrations (≤10 wt%) had smaller average particle sizes (~250-350 nm, PdI~ 0.15-0.300) due to less association of micelles resulting in poorer stabilization of larger nanoplatelets. Higher surfactant concentrations (>10 wt%) form multilayer adsorption of micelles on the nanoplatelet surface enabling the stabilization of large nanoplatelets (~400-500 nm, PdI~0.03).

Both methods are capable of producing nanoplatelets with few-layers to multilayers but ultrasonication demonstrated a greater ability to generate near monolayer nanoplatelets. However, ultrasonication produced a larger range of nanoplatelet thickness than shear mixing. Using TEM and AFM, the resulting GNPs were determined to have aspect ratios of 7-108 and 21-92 in ultrasonication and shear exfoliation systems, respectively.

The scale-up of graphite exfoliation processes that could meet the demands for commercial applications still remains a big challenge. Of the many methods proposed, liquid phase exfoliation through shear mixing can meet this challenge, as it offers the ability to produce high concentrations of graphene nanoplatelets with the potential to be scaled-up to industrial levels. Above a minimum rotor speed, the parameters lay on a relatively simple master curve, which can be applied to larger scale systems. On the other hand, ultrasonication is not scalable, in spite of the fact that it can also produce high concentrations of graphene nanoplatelets.

5.2 Future Work

This work produced some intricate findings with respect to the use of Pluronic® F127. At high concentrations and high amplitudes in ultrasonication, a drastic increase in graphene nanoplatelet concentration was observed. The result was unexpected with unknown exact cause. It is possible that the viscosity of the system is affecting the exfoliation process. This hypothesis can be easily tested using thickeners to increase the viscosity of the system at lower surfactant concentrations. If nanoplatelet concentrations are comparable to what was observed in this work, then further studies should be conducted on the effect of viscosity on the exfoliation method to explain the

increased nanoplatelet concentration. Higher nanoplatelet concentrations are desirable and remain the penultimate goal of liquid phase exfoliation research.

Furthermore, the sequential addition of surfactant lacks significant research as the current amount of data is unable to explain the increase in nanoplatelet concentration over batch experiments. Based on batch exfoliation data, one would expect to observe smaller nanoplatelet concentrations in sequential addition since the surfactant concentration in the system is, on average, lower than batch systems. Studying the effects of sequential addition at other amplitudes and more surfactant concentrations can provide insight to the reason behind an increase in nanoplatelet concentration. Optimizing this process can provide higher nanoplatelet concentrations leading to better production rates.

The size of the initial graphite material is also a matter of concern where starting with graphite particle sizes on the micrometer scale may provide better results. It is possible that less time would be required to breakdown the bulk material to the nanoplatelet sizes obtained in this thesis. Thus, the process would be more devoted to the exfoliation of MLG to FLG and provide a system with more FLG on average. Additionally, the exfoliation of the GNPs should be investigated to determine the applicability of utilizing a stepwise process for better production of FLGs. It was shown that higher amplitudes are more likely to promote cleavage exfoliation mechanisms while at lower amplitudes *exfoliation* mechanisms are more predominant. Therefore, introducing a processing route where high amplitudes are used to induce high production rates followed by a reduction in amplitude to promote *exfoliation* mechanisms may result in higher production rates of FLG. FLG are advantageous over MLG due to better aspect ratios which in turn are more applicable as strengthening fillers in polymers. Thus, production

methods that efficiently produce high concentrations of FLG are desirable for industrial applications.

Regarding the scale-up of liquid phase exfoliation via shear mixing, more experimental conditions are required. Specifically, varying the volume, initial graphite concentration, and rotor diameter should be investigated. Larger volumes increase the production rate but it is unknown if the exfoliation is efficient under larger loads. Additionally, starting with a higher initial graphite concentration could generate larger production rates simply due to more processable material. However, the limit of this parameter is unknown and using higher graphite concentrations may be unnecessary. Lastly, the rotor diameter has a direct influence on the shear rate of the system. Larger diameters increase the shear rate and increased shear rates produce higher concentrations of graphene nanoplatelets. Combining all the parameters in the dimensional analysis are necessary for trustworthy scale-up relationships.

References

[1] Y. Huang, J. Liang and Y. Chen, "An Overview of the Applications of Graphene-Based Materials in Supercapacitors," *Small,* vol. 8, no. 12, pp. 1805-1834, 2012.

[2] J. Liang, Y. Huang, L. Zhang, Y. Wang, Y. Ma, T. Guo and Y. Chen, "Molecular-Level Dispersion of Graphene into Poly(vinyl alcohol) and Effective Reinforcement of their Nanocomposites," *Advanced Functional Materials,* vol. 19, pp. 1-6, 2009.

[3] S. Stankovich, D. A. Dikin, G. Dommett, K. M. Kohlhaas, E. J. Zimney, E. A. Stach, R. D. Piner, S. T. Nguyen and R. S. Ruoff, "Graphene-based composite materials," *Nature,* vol. 442, pp. 282-286, 2006.

[4] X. Wang, Y. Gu, Z. Xiong, Z. Cui and T. Zhang, "Silk-Molded Flexible, Ultrasensitive, and Highly Stable Electronic Skin for Monitoring Human Physiological Signals," *Advanced Materials,* vol. 26, pp. 1336-1342, 2014.

[5] Q. He, H. G. Sudibya, Z. Yin, S. Wu, H. Li, F. Boey, W. Huang, P. Chen and H. Zhang, "Centimeter-Long and Large-Scale Micropatterns of Reduced Graphene Oxide Films: Fabrication and Sensing Applications," *ACS Nano,* vol. 4, no. 6, pp. 3201-3208, 2010.

[6] F. Schedin, A. K. Geim, S. V. Morozov, E. W. Hill, P. Blake, M. I. Katsnelson and K. S. Novoselov, "Detection of individual gas molecules adsorbed on graphene," *Nature Materials,* vol. 6, pp. 652-655, 2007.

[7] B. Li, X. Cao, H. G. Ong, J. W. Cheah, X. Zhou, Z. Yin, H. Li, J. Wang, F. Boey, W.

Huang and H. Zhang, "All-Carbon Electronic Devices Fabricated by Directly Grown Single-Walled Carbon Nanotubes on Reduced Graphene Oxide Electrodes," *Advanced Materials,* vol. 22, pp. 3058-3061, 2010.

[8] A. Das, S. Pisana, B. Chakraborty, S. Piscanec, S. K. Saha, U. V. Waghmare, K. S. Novoselov, H. R. Krishnamurthy, A. K. Geim, A. C. Ferrari and A. K. Sood, "Monitoring dopants by Raman scattering in an electrochemically top-gated graphene transistor," *Nature Nanotechnology,* vol. 3, pp. 210-215, 2008.

[9] J. R. Potts, D. R. Dreyer and C. R. R. S. Bielawski, "Graphene-based polymer nanocomposites," *Polymer,* vol. 52, pp. 5-25, 2011.

[10] T. Premkumar and K. E. Geckeler, "Graphene–DNA hybrid materials Assembly, applications, and prospects," *Progress in Polymer Science,* vol. 37, pp. 515-529, 2012.

[11] C. I. G. A. R. Justino, A. C. Freitas, A. C. Duarte and T. A. Rocha-Santos, "Graphene based sensors and biosensors," *Trends in Analytical Chemistry,* vol. 91, pp. 53-66, 2017.

[12] H. Shen, L. Zhang, M. Liu and Z. Zhang, "Biomedical Applications of Graphene," *Theranostics,* vol. 2, no. 3, pp. 283-294, 2012.

[13] Cohen-Karni, Tzahi, Q. Qing, Q. Li, Y. Fang and C. M. Lieber, "Graphene and Nanowire Transistors for Cellular Interfaces and Electrical Recording," *Nano Letters,* vol. 10, no. 3, pp. 1098-1102, 2010.

[14] Z. Chen, D. Yu, W. Xiong, P. Liu, Y. Liu and L. Dai, "Graphene-Based Nanowire

Supercapacitors," *Langmuir,* vol. 30, pp. 3567-3571, 2014.

[15] A. Yu, I. Roes, A. Davies and Z. Chen, "Ultrathin, transparent, and flexible graphene films for supercapacitor," *Applied Physics Letters,* vol. 96, p. 253105, 2010.

[16] S. R. C. Vivekchand, C. S. Rout, K. S. Subrahmanyam, A. Govindaraj and R. C. N. R, "Graphene-based electrochemical supercapacitors," *Journal of Chemical Science,* vol. 120, no. 1, pp. 9-13, 2008.

[17] J. M. Tour, "Top-Down versus Bottom-Up Fabrication of Graphene-Based Electronics," *Chemistry of Materials,* vol. 26, pp. 163-171, 2014.

[18] S. A. Bhuyan, N. Uddin, M. Islam, F. A. Bipasha and S. S. Hossain, "Synthesis of Graphene," *International Nano Letters,* vol. 6, no. 2, pp. 65-83, 2016.

[19] H. Tetlow, J. Posthuma de Boer, I. J. Ford, D. D. Vvedensky, J. Coraux and L. Kantorovich, "Growth of epitaxial graphene: Theory and experiment," *Physics Reports,* vol. 542, pp. 195-295, 2014.

[20] C. Miao, C. Zheng, O. Liang and Y.-H. Xie, "Chemical Vapor Deposition of Graphene," in *Physics and Applications of Graphene - Experiments*, Rijeka, InTech, 2011, pp. 37-54.

[21] K. S. Novoselov, A. K. Geim, S. V. Morozov, D. Jiang, Y. Zhang, S. V. Dubonos, I. V. Grigorieva and A. A. Firsov, "Electric Field Effect in Atomically Thin Carbon Films," *Science,* vol. 306, pp. 666-669, 2004.

[22] Y. H. Wu and Z. X. Shen, "Two-dimensional carbon nanostructures: Fundamental

properties, synthesis, characterization, and potential applications," *Applied Physics Reviews,* vol. 108, p. 071301, 2010.

[23] K. S. Novoselov, D. Jiang, F. Schedin, T. J. Booth, K. V. V, S. V. Morozov and A. K. Geim, "Two-dimensional atomic crystals," *PNAS,* vol. 102, no. 30, pp. 10451-10453, 2005.

[24] A. K. Geim and K. S. Novoselov, "The rise of graphene," *Nature Materials,* vol. 6, pp. 183-191, 2007.

[25] F. Bonaccorso, "Graphene, related two-dimensional crystals, and hybrid systems for energy conversion and storage," *Science,* vol. 347, no. 6217, pp. 41-51, 2015.

[26] C. Lee, X. K. J. W. Wei and J. Hone, "Measurement of the Elastic Properties and Intrinsic Strength of Monolayer Graphene," *Science,* vol. 321, pp. 385-388, 2008.

[27] K. I. Bolotin, K. J. Sikes, Z. Jiang, M. Klima, G. Fudenberg, J. Hone, P. Kim and H. L. Stormer, "Ultrahigh electron mobility in suspended graphene," *Solid State Communications,* vol. 146, pp. 351-355, 2008.

[28] A. H. Castro Neto, F. Guinea, N. M. R. Peres, K. S. Novoselov and A. K. Geim, "The electronic properties of graphene," *Reviews of Modern Physics,* vol. 81, no. 1, pp. 109-162, 2009.

[29] N. Peres, "Colloquim: The transport properties of graphene: An introduction," *Reviews of Modern Physics,* vol. 82, no. 3, pp. 2673-2700, 2010.

[30] A. S. Mayorov, D. C. Elias, I. S. Mukhin, S. V. Morozov, L. A. Ponomarenko, K. S. Novoselov, A. K. Geim and R. V. Gorbachev, "How Close Can One Approach the Dirac Point in Graphene Experimentally?," *Nano Letters,* vol. 12, pp. 4629-4634, 2012.

[31] A. A. Balandin, "Thermal properties of graphene and nanostructured carbon materials," *Nature Materials,* vol. 10, pp. 569-581, 2011.

[32] E. Pop, V. Varshney and A. K. Roy, "Thermal properties of graphene: Fundamentals and applications," *Materials Research Society,* vol. 37, pp. 1273-1281, 2012.

[33] F. Rozploch, J. Patyk and J. Stankowski, "Graphenes Bonding Forces in Graphite," *Acta Physica Polonica,* p. 112, 2007.

[34] J. C. Charlier, X. Gonze and J. P. Michenaud, "Graphite Interplanar Bonding: Electronic Delocalization and van der Waals Interaction," *Europhysics Letters,* vol. 28, no. 6, pp. 403-408, 1994.

[35] J. C. Charlier, X. Gonze and J. P. Michenaud, "First-principles study of the electronic properties of graphite," *Physical Review,* vol. 43, no. 6, pp. 4579-4589, 1991.

[36] T. Gould, Z. Liu, J. Z. Liu, J. F. Dobson, Q. Zheng and S. Lebeque, "Binding and interlayer force in the near-contact region of two graphite slabs: Experiment and theory," *Journal of Chemical Physics,* vol. 139, p. 224704, 2013.

[37] W. Wang, S. Dai, X. Li, J. Yang, D. J. Srolovitz and Q. Zheng, "Measurement of the cleavage energy of graphite," *Nature Communications,* vol. 6, p. 7853, 2015.

[38] T. Bjorkman, A. Gulans, A. V. Krasheninnikov and R. M. Nieminen, "Van der Waals Bonding in Layered Compounds from Advanced Density-Functional First-Principles Calculations," *Physical Review Letters,* vol. 108, p. 235502, 2012.

[39] Z. Liu, J. Z. Liu, Y. Cheng, Z. Li, L. Wang and Z. Quanshui, "Interlayer binding energy of graphite: A mesoscopic determination from deformation," *Physical Review,* vol. 85, p. 205418, 2012.

[40] Y. Hernandez, V. Nicolosi, M. Lotya, F. M. Blighe, Z. Sun, S. De, I. T. Mcgovern, B. Holland, M. Byrne, Y. K. Gun'ko, J. J. Boland, P. Niraj, G. Duesberg, S. Krishnamurthy, R. Goodhue, J. Hutchinson, V. Scardaci, A. C. Ferrari and J. N. Coleman, "High-yield production of graphene by liquid-phase exfoliation of graphite," *Nature Nanotechnology,* vol. 3, pp. 563-568, 2008.

[41] G. Eda, G. Fanchini and M. Chhowalla, "Large-area ultrathin films of reduced graphene oxide as a transparent and flexible electronic material," *Nature Nanotechnology,* vol. 3, pp. 270-274, 2008.

[42] D. Li, M. B. Muller, S. Gilje, R. B. Kaner and G. G. Wallace, "Processable aqueous dispersions of graphene nanosheets," *Nature Nanotechnology,* vol. 3, pp. 101-105, 2008.

[43] X. Wang, L. Zhi and K. Mullen, "Transparent, Conductive Graphene Electrodes for Dye-Sensitized Solar Cells," *Nano Letters,* vol. 8, no. 1, pp. 323-327, 2008.

[44] S. N. Alam, N. Sharma and L. Kumar, "Synthesis of Graphene Oxide (GO) by Modified Hummers Method and Its Thermal Reduction to Obtain Reduced Graphene Oxide (rGO),"

Graphene, vol. 6, no. 1, pp. 1-18, 2017.

[45] S. Niyogi, E. Bekyarova, M. E. Itkis, J. L. McWilliams, M. A. Hamon and R. C. Haddon, "Solution Properties of Graphite and Graphene," *Journal of American Chemical Society,* vol. 128, pp. 7720-7721, 2006.

[46] D. C. Marcano, D. V. Kosynkin, J. M. Berlin, A. Sinitskii, Z. Sun, A. Slesarev, L. B. Alemany, W. Lu and J. M. Tour, "Improved Synthesis of Graphene Oxide," *ACS Nano,* vol. 4, no. 8, pp. 4806-4814, 2010.

[47] B. Paulchamy, G. Arthi and B. Lignesh, "A Simple Approach to Stepwise Synthesis of Graphene Oxide Nanomaterial," *Nanomedicine & Nanotechnology,* vol. 6, no. 1, p. 1000253, 2015.

[48] H. Yu, B. Zhang, C. Bulin, R. Li and R. Xing, "High-efficient Synthesis of Graphene Oxide Based on Improved Hummers Method," *Scientific Reports,* vol. 6, p. 36143, 2016.

[49] S. Stankovich, R. D. Piner, X. Chen, N. Wu, S. T. Nguyen and R. S. Ruoff, "Stable aqueous dispersions of graphitic nanoplatelets via the reduction of exfoliated graphite oxide in the presence of poly sodium 4-styrenesulfonate," *Journal of Materials Chemistry,* vol. 16, pp. 155-158, 2006.

[50] S. Stankovich, D. A. Dikin, R. D. Piner, K. a. Kohlhaas, A. Kleinhammes, Y. Jia, Y. Wu, S. T. Nguyen and R. S. Ruoff, "Synthesis of graphene-based nanosheets via chemical reduction of exfoliated graphite oxide," *Carbon,* vol. 45, pp. 1558-1565, 2007.

[51] C. Gomez-Navarro, R. T. Weitz, A. M. Bittner, M. Scolari, A. Mews, M. Burghard and K.

Kern, "Electronic Transport Properties of Individual Chemically Reduced Graphene Oxide Sheets," *Nano Letters,* vol. 7, no. 11, pp. 3499-3503, 2007.

[52] C. Gomez-Navarro, J. C. Meyer, R. S. Sundaram, A. Chuvilin, S. Kurasch, M. Burghard, K. Kern and U. Kaiser, "Atomic Structure of Reduced Graphene Oxide," *Nano Letters,* vol. 10, pp. 1144-1148, 2010.

[53] G. Williams, B. Seger and P. V. Kamt, "TiO2 - Graphene Nanocomposites. UV-Assisted Photocatalytic Reduction of Graphene Oxide," *ACS Nano,* vol. 2, no. 7, pp. 1487-1491, 2008.

[54] U. Khan, A. O'Neill, M. Lotya, S. De and J. N. Coleman, "High-Concentration Solvent Exfoliation of Graphene," *Small,* vol. 7, pp. 864-871, 2010.

[55] M. J. McAllister, J.-L. Li and D. H. Adamson, "Single Sheet Functionalized Graphene by Oxidation and Thermal Expansion of Graphite," *Chemistry of Materials,* vol. 19, no. 18, pp. 4396-4404, 2007.

[56] H. A. Becerril, J. Mao, Z. Liu, R. M. Stoltenberg, Z. Bao and Y. Chen, "Evaluation of Solution-Processed Reduced Graphene Oxide Films as Transparent Conductors," *ACS Nano,* vol. 2, no. 3, pp. 463-470, 2008.

[57] S. D. Bergin, V. Nicolosi, P. V. Streich, S. Girodani, Z. Sun, A. H. Windle, P. Ryan, P. P. Niraj, Z.-T. T. Wang, L. Carpenter, W. J. Blau, J. J. Boland, J. P. Hamilton and J. N. Coleman, "Towards Solutions of Single-Walled Carbon Nanotubes in Common Solvent," *Advanced Materials,* vol. 20, pp. 1876-1881, 2008.

[58] K. R. Paton, E. Varrla, C. Backes, R. J. Smith, U. Khan, A. O'Neill, C. Boland, M. Lotya, O. M. Istrate, P. King, T. Higgins, S. Barwich, P. May, P. Puczkarski, I. Ahmed, M. Moebius, H. Pettersson, E. Long, J. Coelho, S. E. O'Brien, E. K. McGuire, B. M. Sanchez, G. S. Duesberg, N. McEvoy and T. J. Pennycook, "Scalable production of large quantities of defect-free few-layer graphene by shear exfoliation in liquids," *Nature Materials,* vol. 13, no. 6, pp. 624-630, 2014.

[59] P. G. Karagiannidis, S. A. Hodge, L. Lombardi, F. Tomarchio, N. Decorde, S. Milana, I. Goykhman, Y. Su, S. V. Mesite, D. N. Johnstone, R. K. Leary, P. A. Midgley, N. M. Pugno, F. Torrisi and A. C. Ferrari, "Microfluidization of Graphite and Formulation of Graphene-Based Conductive Inks," *ACS Nano,* vol. 11, no. 3, pp. 2742-2755, 2017.

[60] M. Lotya, P. J. King, U. Khan, S. De and J. N. Coleman, "High-Concentration Surfactant-Stabilized Graphene Dispersions," *ACS Nano,* vol. 4, no. 6, pp. 3155-3162, 2010.

[61] Z. Sun, J. Masa, Z. Liu, W. Schuhmann and M. Muhler, "Highly Concentrated Aqueous Dispersions of Graphene Exfoliated by Sodium Taurodeoxycholate: Dispersion Behavior and Potential Application as a Catalyst Support for the Oxygen-Reduction Reaction," *Chemistry,* vol. 18, pp. 6972-6978, 2012.

[62] S. M. Notley, "Highly Concentrated Aqueous Suspensions of Graphene through Highly Concentrated Aqueous Suspensions of Graphene through," *Langmuir,* vol. 28, pp. 14110-14113, 2012.

[63] S. Pilli, P. Bhunia, S. Yan, R. J. LeBlanc, R. D. Tyagu and R. Y. Surampalli, "Ultrasonic

pretreatment of sludge: A review," *Ultrasonics Sonochemistry,* vol. 18, pp. 1-18, 2011.

[64] N. K. Rastogi, "Opportunities and Challenges in Application of Ultrasound in Food Processing," *Critical Reviews in Food Science and Nutrition,* vol. 51, no. 8, pp. 705-722, 2011.

[65] T. I. Onyeche, O. Schlafer, H. Bormann, C. Schroder and M. Sievers, "Ultrasonic cell disruption of stabilised sludge with subsequent anaerobic digestion," *Ultrasonics,* vol. 40, pp. 31-35, 2002.

[66] K. S. Suslick, "Sonochemistry," *Science,* vol. 247, pp. 1439-1445, 1990.

[67] E. B. Flint and K. S. Suslick, "The Temperature of Cavitation," *Science,* vol. 253, pp. 1397-1399, 1991.

[68] S. Haar, M. Bruna, J. X. Lian, F. Tomarchio, Y. Olivier, R. Mazzaro, V. Morandi, J. Moran, A. C. Ferarri, D. Beljonne, A. Ciesielski and P. Samori, "Liquid-Phase Exfoliation of Graphite into Single- and Few-Layer Graphene with α-Functionalized Alkanes," *Journal of Physical Chemistry Letters,* vol. 7, pp. 2714-2721, 2016.

[69] C. Backes, T. M. Higgins, A. Kelly, C. Boland, A. Harvey, H. Damien and J. N. Coleman, "Guidelines for Exfoliation, Characterization and Processing of Layered Materials Produced by Liquid Exfoliation," *Chemistry of Materials,* vol. 29, pp. 243-255, 2017.

[70] A. S. Pavlova, E. A. Obraztsova, A. V. Belkin, C. Monat, P. Rojo-Romeo and E. D. Obraztsova, "Liquid-phase exfoliation of flaky graphite," *Journal of Nanophotonics,* vol.

10, no. 1, p. 012525, 2016.

[71] Z. Lin, P. S. Karthik, M. Hada, T. Nishikawa and Y. Hayashi, "Simple Technique of Exfoliation and Dispersion of Multilayer Graphene from Natural Graphite by Ozone-Assisted Sonication," *Nanomaterials,* vol. 7, no. 6, p. 125, 2017.

[72] R. Narayan and S. O. Kim, "Surfactant mediated liquid phase exfoliation of graphene," *Nano Convergence,* vol. 2, no. 1, 2015.

[73] A. Ciesielski and P. Samori, "Graphene via sonication assisted liquid-phase exfoliation," *Chemical Society Reviews,* vol. 43, no. 1, pp. 381-398, 2014.

[74] D. R. Devi, P. Sandhya and B. V. Hari, "Poloxamer: A Novel Functional Molecule For Drug Delivery And Gene Therapy," *Journal of Pharmaceutical Sciences and Research,* vol. 5, no. 8, pp. 159-165, 2013.

[75] A. V. Kabanov, P. Lemieux, S. Vinogradov and V. Alakhov, "Pluronic block copolymers: novel functional molecules for gene therapy," *Advanced Drug Delivery Reviews,* vol. 54, pp. 222-233, 2002.

[76] H. R. Patel, R. P. Patel and M. M. Patel, "Poloxamers: A pharmaceutical excipients with therapeutic behaviors," *International Journal of PharmTech Research,* vol. 1, no. 2, pp. 299-303, 2009.

[77] L. Guardia, Fernandex-Merino, J. I. Paredes, P. Solis-Fernandez, S. Villar-Rodil, A. Martinez-Alonso and J. M. D. Tascon, "High-throughput production of pristine graphene in an aqueous dispersion assisted by non-ionic surfactants," *Carbon,* vol. 49, pp. 1653-

1662, 2011.

[78] F. Aydin, X. Chu, G. Uppaladadium, D. Devore, R. Goyal, N. S. Murthy, Z. Zhang, J. Kohn and M. Dutt, "Self-Assembly and Critical Aggregation Concentration Measurements of ABA Triblock Copolymers with Varying B Block Types: Model Development, Prediction, and Validation," *Journal of Physical Chemistry,* vol. 120, pp. 3666-3676, 2016.

[79] Y. Lin and P. Alexandridis, "Temperature-Dependent Adsorption of Pluronic F127 Block Copolymers onto Carbon Black Particles Dispersed in Aqueous Media," *Journal of Physical Chemistry,* vol. 106, pp. 10834-10844, 2002.

[80] F. Miano, A. Bailey, P. F. Luckham and T. F. Tadros, "Adsorption of ploy(ethylene oxide)-poly(propylene oxide) ABA block copolymers on carbon black and the rheology of the resulting dispersions," *Colloids and Surfaces,* vol. 68, pp. 9-16, 1992.

[81] S. Stolnik, B. Daudali, A. Arien, J. Whetstone, C. R. Heald, M. C. Garnett, S. S. David and L. Illum, "The effect of surface coverage and conformation of poly(ethylene oxide) (PEO) chains of poloxamer 407 on the biological fate of model colloidal drug carriers," *Biochimica et Biophysica Acta,* vol. 1514, no. 2, pp. 261-279, 2001.

[82] K.-H. Liao, A. Mittal, S. Bose, C. Leighton, K. A. Mkhoyan and C. W. Macosko, "Aqueous Only Route toward Graphene from Graphite Oxide," *ACS Nano,* vol. 5, no. 2, pp. 1253-1258, 2011.

[83] X. Geng, Y. Guo, D. Li, W. Li, C. Zhu, X. Wei, M. Chen, S. Gao, S. Qiu, Y. Gong, L. Wu, M. Long, M. Sun, G. Pan and L. Liu, "Interlayer catalytic exfoliation realizing scalable

production of large-size pristine few-layer graphene," *Scientific Reports,* vol. 3, p. 1134, 2013.

[84] H. Feng, R. Cheng, X. Zhao, X. Duan and J. Li, "A low-temperature method to produce highly reduced graphene oxide," *Nature Communications,* vol. 4, p. 1539, 2013.

[85] W. Lu, S. Liu, X. Qin, L. Wang, J. Tian, Y. Luo, A. M. Asiri, A. O. Al-Youbi and X. Sun, "High-yield, large-scale production of few-layer graphene flakes within seconds: using chlorosulfonic acid and H2O2 as exfoliating agents," *Journal of Materials Chemistry,* vol. 22, pp. 8775-8777, 2012.

[86] D. Parviz, S. Das, H. S. T. Ahmed, F. Irin, S. Bhattacharia and M. J. Green, "Dispersions of Non-Covalently Functionalized Graphene with Minimal Stabilizer," *ACS Nano,* vol. 6, pp. 8857-8867, 2012.

[87] A. A. Green and M. C. Hersam, "Solution Phase Production of Graphene with Controlled Thickness via Density Differentiation," *Nano Letters,* vol. 9, no. 12, pp. 4031-4036, 2009.

[88] R. J. Smith, M. Lotya and J. N. Coleman, "The importance of repulsive potential barriers for the dispersion of graphene using surfactants," *New Journal of Physics,* vol. 12, p. 125008, 2010.

[89] R. Wengeler and H. Nirschl, "Turbulent hydrodynamic stress induced dispersion and fragmentation of nanoscale agglomerates," *Colloid and Interface Science,* vol. 306, pp. 262-273, 2007.

[90] D. W. Murphy and G. W. Hull Jr., "Monodispersed tantalum disulfide and adsorption

complexes with cations," *Journal of Chemical Physics,* vol. 62, no. 3, pp. 973-978, 1975.

[91] G. F. Walker and G. W. G, "Chemical exfoliation of vermiculite and production of colloidal dispersions," *Science,* vol. 156, pp. 385-387, 1967.

[92] J. Guo, "Low-temperature method of producing nano-scaled graphene platelets and their nanocomposites". United States of America Patent 20,080,258,359, 23 October 2008.

[93] U. Khan, H. Porwal, A. O'Neill, K. Nawaz, P. May and J. N. Coleman, "Solvent-Exfoliated Graphene at Extremely High Concentration," *Langmuir,* vol. 27, pp. 9077-9082, 2011.

[94] M. Monajjemi, "Liquid-phase exfoliation (LPE) of graphite towards graphene: An ab initio study," *Journal of Molecular Liquids,* vol. 230, pp. 461-472, 2017.

[95] M. P. Lavin-Lopez, J. L. Valverde, L. Sanchez-Silva and A. Romero, "Solvent-Based Exfoliation via Sonication of Graphitic Materials for Graphene Manufacture," *Industrial & Engineering Chemistry Research,* vol. 55, no. 4, pp. 845-855, 2016.

[96] T. Lin, Y. Tang, Y. Wang, H. Bi, Z. Liu, F. Huang, X. Xie and M. Jiang, "Scotch-tape-like exfoliation of graphite assisted with elemental sulfur and graphene high-performance lithium-sulfur batteries," *Energy & Environmental Science,* vol. 6, pp. 1283-1290, 2013.

[97] Y. Hernandez, M. Lotya, D. Rickard, S. D. Bergin and J. N. Coleman, "Measurement of Multicomponent Solubility Parameters for Graphene Facilitates Solvent Discovery," *Langmuir,* vol. 26, no. 5, pp. 32088-3213, 2010.

[98] E.-Y. Choi, W. S. Choi, Y. B. Lee and Y.-Y. Noh, "Production of graphene by exfoliation

of graphite in a volatile organic solvent," *Nanotechnology,* vol. 22, no. 36, p. 365601, 2011.

[99] M. Lotya, P. J. King, U. Khan, S. De and J. N. Coleman, "High-Concentration, Surfactant-Stabilized Graphene Dispersions," *ACS Nano,* vol. 4, no. 6, pp. 3155-3162, 2010.

[100] S. Tanaka, Y. Katayama, M. P. Tate, H. W. Hillhouse and Y. Miyake, "Fabrication of continuous mesoporous carbon films with face-centered orthorhombic symmetry through a soft templating pathway," *Journal of Materials Chemistry,* vol. 17, pp. 3639-3645, 2007.

[101] L. Liu, S. Ryu, M. R. Tomasik, E. Stolyarova, N. Jung, M. S. Hybertsen, M. L. Steigerwald, L. E. Brus and G. W. Flynn, "Graphene Oxidation: Thickness-Dependent Etching and Strong Chemical Doping," *Nano Letters,* vol. 8, no. 7, pp. 1965-1970, 2008.

[102] L. Xiaowei, R. Jean-Charles and Y. Suyuan, "Effect of temperature on graphite oxidation behavior," *Nuclear Engineering and Design,* vol. 227, pp. 273-280, 2004.

[103] E. A. Gulbransen, K. F. Andrew and F. A. Brassart, "The Oxidation of Graphite at Temperatures of 600 to 1500C and at Pressures of 2 to 76 Torr of Oxygen," *Journal of the Electrochemical Society,* vol. 110, no. 6, pp. 476-483, 1963.

[104] S. Wang, M. Yi and Z. Shen, "The effect of surfactants and their concentration on the liquid exfoliation of graphene," *RCS Advances,* vol. 6, p. 56705, 2016.

[105] J. Fan, Z. Shi, Y. Ge, J. Wang, Y. Wang and J. Yin, "Gum arabic assisted exfoliation and fabrication of Ag–graphene-based hybrids," *Journal of Materials Chemistry,* vol. 22, p.

13764, 2012.

[106] R. Su, L. S. Fen, D. Q. Chen and G. H. Chen, "Study on the Absorption Coefficient of Reduced Graphene Oxide Dispersion," *Journal of Physical Chemistry,* vol. 118, pp. 12520-12525, 2014.

[107] A. S. Wajid, S. Das, F. Irin, H. T. Ahmed, J. L. Shelburne, D. Parviz, R. J. Fullerton, A. F. Jankowski, R. C. Hedden and M. J. Greeen, "Polymer-stabilized graphene dispersions at high concentrations in organic solvents for composite production," *Carbon,* vol. 50, pp. 526-534, 2012.

[108] Malvern, "Dynamic Light Scattering Common Terms Defined," Malvern Instruments Limited, Worcestershire, 2011.

[109] U. Nobbmann, "Polydispersity – what does it mean for DLS and chromatography?," Malvern, 23 October 2014. [Online]. Available: http://www.materials-talks.com/blog/2014/10/23/polydispersity-what-does-it-mean-for-dls-and-chromatography/. [Accessed 15 September 2017].

[110] Y. Zhang and Y. Lam, "Controlled synthesis and association behavior of graft Pluronic in aqueous solutions," *Colloid and Interface Science,* vol. 306, pp. 398-404, 2007.

[111] Y. R. Jang, K. Y. Kin and K. H. Yoo, "Accurate measurement of thickness of large-area graphene layers by neutron reflectometry," *Journal of Material Science,* vol. 51, pp. 10059-10065, 2016.

[112] Y. Baskin and L. Meyer, "Lattice Constants of Graphite at Low Temperatures," *Physical*

Review, vol. 100, no. 2, p. 544, 1955.

[113] W. Wei and X. Qu, "Extraordinary Physical Properties of Functionalized Graphene," *Small,* vol. 8, no. 14, pp. 2138-2151, 2012.

[114] A. Ghosh, K. S. Subrahmanyam, K. S. Krishna, S. Datta, A. Govindaraj, S. K. Pati and C. Rao, "Uptake of H2 and CO2 by Graphene," *Journal of Physical Chemistry,* vol. 112, no. 40, pp. 15704-15707, 2008.

[115] S. Gayathri, P. Jayabal, M. Kottaisamy and V. Ramakrishnan, "Synthesis of few layer graphene by direct exfoliation of graphite and a Raman spectroscopic study," *AIP Advances,* vol. 4, p. 027116, 2014.

[116] T. Gould, G. Evan and J. F. Dobson, "van der Waals dispersion power laws for cleavage, exfoliation, and stretching in multiscale, layered systems," *Physical Review,* vol. 79, p. 113402, 2009.

[117] M. Jalaal, G. Cottrell, N. Balmforth and B. Stoeber, "On the rheology of Pluronic F127 aqueous solutions," *Journal of Rheology,* vol. 61, pp. 139-146, 2017.

[118] A. El-Kamel, "In vitro and in vivo evaluation of Pluronic F127-based ocular delivery system for timolol maleate," *International Journal of Pharmaceutics,* vol. 241, pp. 47-55, 2002.

[119] S. C. Miller and B. R. Drabik, "Rheological properties of poloxamer vehicles," *International Journal of Pharmaceutics,* vol. 18, pp. 269-276, 1984.

[120] F. Tirnaksiz and J. Robinson, "Rheological, mucoadhesive and release properties of Pluronic F-127 gel and Pluronic F-127/polycarbophil mixed gel systems," *Pharmazie,* vol. 60, pp. 518-523, 2005.

[121] M. R. Nejadnik, A. L. J. Olsson, P. K. Sharma, H. C. van der Mei, W. Norde and H. J. Busscher, "Adsorption of Pluronic F-127 on Surfaces with Different Hydrophobicities Probed by Quartz Crystal Microbalance with Dissipation," *Langmuir,* vol. 25, no. 11, pp. 6245-6249, 2009.

[122] Y. Lin, T. W. Smith and P. Alexandridis, "Adsorption of Amphiphilic Copolymers on Hydrophobic Particles in Aqueous Media," *Journal of Dispersion Science and Technology,* vol. 23, no. 4, pp. 539-553, 2002.

[123] E. S. Kastrisianaki-Guyton, L. Chen, S. E. Rogers, T. Cosgrove and J. S. van Duijneveldt, "Adsorption of F127 onto Single-Walled Carbon Nanotubes Characterized Using Small-Angle Neutron Scattering," *Langmuir,* vol. 21, pp. 3262-3268, 2015.

[124] Y.-M. G. N. G.-W. G. Lam, "Direct visualisation of micelles of Pluronic block copolymers in aqueous solution by cryo-TEM," *Physical Chemistry Chemical Physics,* vol. 1, no. 14, pp. 3331-3334, 1999.

[125] Q. Yu, J. Lian, S. Siriponglert, H. Li, Y. P. Chen and S.-S. Pei, "Graphene segregated on Ni surfaces and transferred to insulators," *Applied Physics Letters,* vol. 93, p. 113103, 2008.

[126] X. Li, W. Cai, J. An, S. Kim, J. Nah, D. Yang, R. Piner, A. Velamakanni, I. Jung, E. Tutuc,

S. K. Banerjee, L. Colombo and R. S. Ruoff, "Large-Area Synthesis of High-Quality and Uniform Graphene Films on Copper Foils," *Science,* vol. 324, pp. 1312-1314, 2009.

[127] J. Nam, D.-C. Kim, H. Yun, D. H. Shin, S. Nam, W. K. Lee, J. Y. Hwang, S. W. Lee, H. Weman and K. S. Kim, "Chemical vapor deposition of graphene on platinum: Growth and substrate interaction," *Carbon,* vol. 111, pp. 733-740, 2017.

[128] T. S. Tran, S. J. Park, S. S. Yoo, T.-R. Lee and T. Kim, "High shear-induced exfoliation of graphite into high quality graphene by Taylor-Couette flow," *RSC Advances,* vol. 6, no. 15, pp. 12003-12008, 2016.

[129] U. Khan, A. O'Neill, H. Porwal, P. May, K. Nawaz and J. N. Coleman, "Size selection of dispersed, exfoliated graphene flakes by controlled centrifugation," *Carbon,* vol. 50, pp. 470-475, 2012.

[130] E. Varrla, K. R. Paton, C. Backes, A. Harvey, R. J. Smith, J. McCauley and J. N. Coleman, "Turbulence-assisted shear exfoliation of graphene using household detergent and a kitchen blender," *Nanoscale,* vol. 6, pp. 11810-11819, 2014.

[131] M. A. Bahri, M. Hoebeke, A. Grammenos, L. Delanaye, N. Vandewalle and A. Seret, "Investigation of SDS, DTAB and CTAB micelle microviscosities by electron spin resonance," *Colloids and Surfaces,* vol. 290, pp. 206-212, 2006.

[132] U. Nobbmann, "PDI from an individual peak in DLS," Malvern, 31 March 2015. [Online]. Available: http://www.materials-talks.com/blog/2015/03/31/pdi-from-an-individual-peak-in-dls/. [Accessed 15 September 2017].

Appendix A: CTAB vs. Pluronic® F127

Preliminary investigations involved testing of one cationic and one non-ionic surfactant, CTAB and Pluronic F127. CTAB was selected based on comparative studies of GNP concentrations in literature and to verify our exfoliation methods. The GNP concentrations obtained by ultrasonication in the presence of these surfactants were measured by UV-VIS spectroscopy and compared. Various concentrations and amplitudes were explored for the two surfactants over the course of a 4-hour sonication. Due to differences in surfactant solubility limits CTAB was studied under much lower concentrations (0.04 wt%) than Pluronic F127 (15 wt%). Both surfactants demonstrated were analyzed using the Lambert-Beer law with an extinction coefficient of 732 $mL \cdot mg^{-1} \cdot m^{-1}$ (λ=660 nm) to determine the GNP concentration. (Figure A.1). In the presence of CTAB, GNP concentrations up to 0.11 mg/mL where produced, whereas Pluronic F127 dispersions resulted in concentrations as high as 3.01 mg/mL. 0.1 wt% Pluronic F127 dispersions exhibited concentrations similar to those of CTAB dispersions (~0.05 mg/mL) after 4-hours under similar conditions (Figure A.1 [131]). Based on these preliminary results, Pluronic F127 was chosen as a more suitable surfactant for the investigations presented in this thesis.

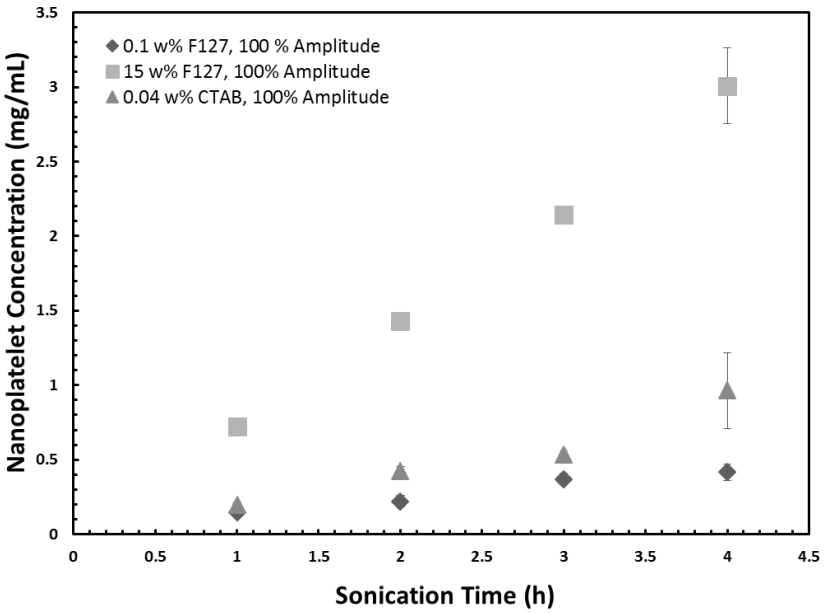

Figure A.1: Batch exfoliation comparing CTAB to Pluronic® F127 at two surfactant concentrations.

Appendix B: Exfoliation via Ultrasonication with Sequential Addition of Surfactant

B.1 Introduction

Ultrasonication-assisted exfoliation of graphite in organic liquids is inherently a batch process. When water is used as the medium, surfactant can be added to the suspension at the beginning of the process, or sequentially. In batch exfoliations operating at CMC, the exfoliation naturally consumes some of the available surfactant through adsorption on the exfoliated platelets; the resulting low surfactant concentration would be susceptible to mass transfer limitations [62]. Notley hypothesized that continuous, or sequential, addition of surfactant during the exfoliation process enables the system to remain close to the critical micelle concentration (CMC) throughout the process, thus resulting in high graphene yields [62]. This Appendix tests this hypothesis by implementing a sequential addition process, based on the exfoliation system described in Chapter 3, under a wide range of processing conditions, to test this hypothesis.

B.2 Experimental Section

B.2.1 Materials

Natural graphite powder (purity 95%) was supplied by Eagle Graphite and purified (99%) with anhydrous ethyl alcohol and acetone. Pluronic® F127 was purchased from Sigma Aldrich and used as received. Milli-Q quality water was used in all of the experiments.

B.2.2 Methods

Graphite (G) was exfoliated using a Microson Ultrasonic Cell Distruptor equipped with a 3 mm diameter sonicating tip. Surfactant concentrations were prepared prior to exfoliation by dissolving Pluronic® F127 in Milli-Q water. Since the dissolution of Pluronic® F127 in water is more favourable at lower temperatures, the mixture was left to equilibrate for 12 h at 4 °C. Graphite powder (3.16 g) was added to Milli-Q water and stirred until adequately mixed. The initial volume of water varied from 15 mL to 60 mL depending on the desired final concentration of surfactant. The final volume was 60 mL in all experiments. The graphite solution was placed in a temperature controlled bath to the maintain temperature at approximately 20 °C (room temperature). Graphite exfoliation was initiated after lowering the sonicating tip halfway down into the solution volume and setting the amplitude between 35 to 100%. The solution was left to exfoliate for 4 hours with addition of surfactant in specified intervals. At final surfactant concentrations of 0.05 and 0.025 wt% surfactant was added every 30 and 60 minutes. For final surfactant concentrations ≤0.1 wt%, surfactant was added every 15 minutes. Stock surfactant concentrations and volume of injections for each experiment are listed in Table B.1. Progression of surfactant concentration in the exfoliating solution is shown in Figure B.1 using the following equation:

$$C_{surfactant} = \frac{V_{injection} N_{injection} C_{stock}}{V_{initial} + V_{injection} N_{injection}} \quad (2)$$

where $C_{surfactant}$ is the concentration of surfactant in the exfoliating solution, $V_{injection}$ is the volume of stock surfactant added per injection, $N_{injection}$ is the number of injections, C_{stock} is the concentration of the stock surfactant solution, and $V_{initial}$ is the intial volume of the exfoliating

solution. Exfoliated samples were taken in 1 hour intervals. These samples were centrifuged at 1800 g for 30 minutes and later used for characterization through ultraviolet-visible spectroscopy (UV-VIS) and dynamic light scattering (DLS).

Table B.1: Conditions of addition of surfactant for various final surfactant concentrations.

Final Surfactant Concentration (wt%)	Stock Solution Concentration (wt%)	Injection Volume (mL)
0.025	4	0.1
0.05	4	0.1
0.1	4	0.1
5	15	1.25
15	20 (cooled below gel point)	2.815

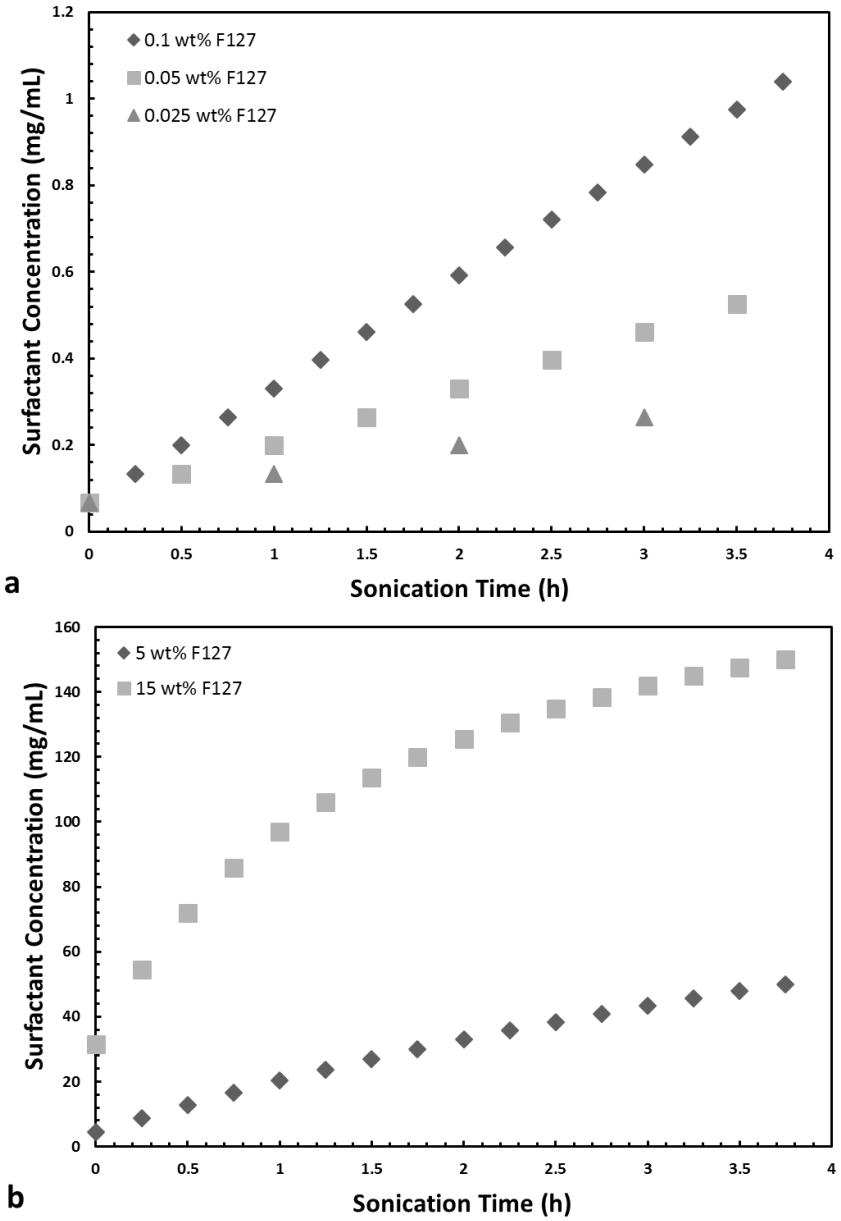

Figure B.1: Progression of surfactant concentration through exfoliation process. (a) Exfoliations performed below CMC. (b) Exfoliations performed above CMC.

B.2.3 Instrumentation and Analysis

UV-VIS spectroscopy was performed on a Varian Cary 100 Scan spectrophotometer. The selected wavelength range was from 400 to 800 nm and the cuvette path length was 0.01 m. Each

sample taken from a 4h exfoliation was measured and the absorbance was converted to concentration using the Lambert-Beer law with an absorption coefficient of 732 $mL \cdot mg^{-1} \cdot m^{-1}$ (λ=660 nm). The supernatants of the centrifuged samples were diluted 10-20 fold to ensure the absorbance was within the instrument's range. The extinction coefficient used in these experiments was determined as described in Chapter 3.

The samples were further diluted (15-fold) with Milli-Q water and estimates of the particle size distribution of the graphene nanoplatelets were obtained through Dynamic Light Scattering (DLS) measurements, using a Malvern Instruments Zetasizer Nano ZS (λ=633 nm). The polydispersity index (PdI) in DLS measurements describes the width of a particle size distribution and is calculated from a Cumulant analysis [108]. Thus, true monodisperse solutions inherently have PdI values of 0. However, the classification of monodisperse ranges from 0.0-0.1 whereas polydisperse ranges from 0.1-0.7 [109]. Values > 0.7 indicate samples that are not suitable for DLS [108]. Data obtained through DLS, however, must be interpreted with caution as the reported particle size, calculated from the Stokes-Einstein equation, is that of the spherical equivalent of GNP. Furthermore, the DLS intensity averages are affected more by larger particles than smaller particles. Thus, it must be taken into account that the larger particles will have a greater affect on the particle size distribution when interpreting the PdI.

B.3 Results

B.3.1 Effect Sequential Addition of Surfactant on GNP Concentration and Size

Similar to the observations made during batch exfoliations, the GNP concentration increases with increasing amplitude however, at extremely low surfactant concentrations this effect is not as significant. (Figure B.2a). Increasing the surfactant concentration resulted in an increase in the GNP concentration, throughout the experiment (Figure B.2b).

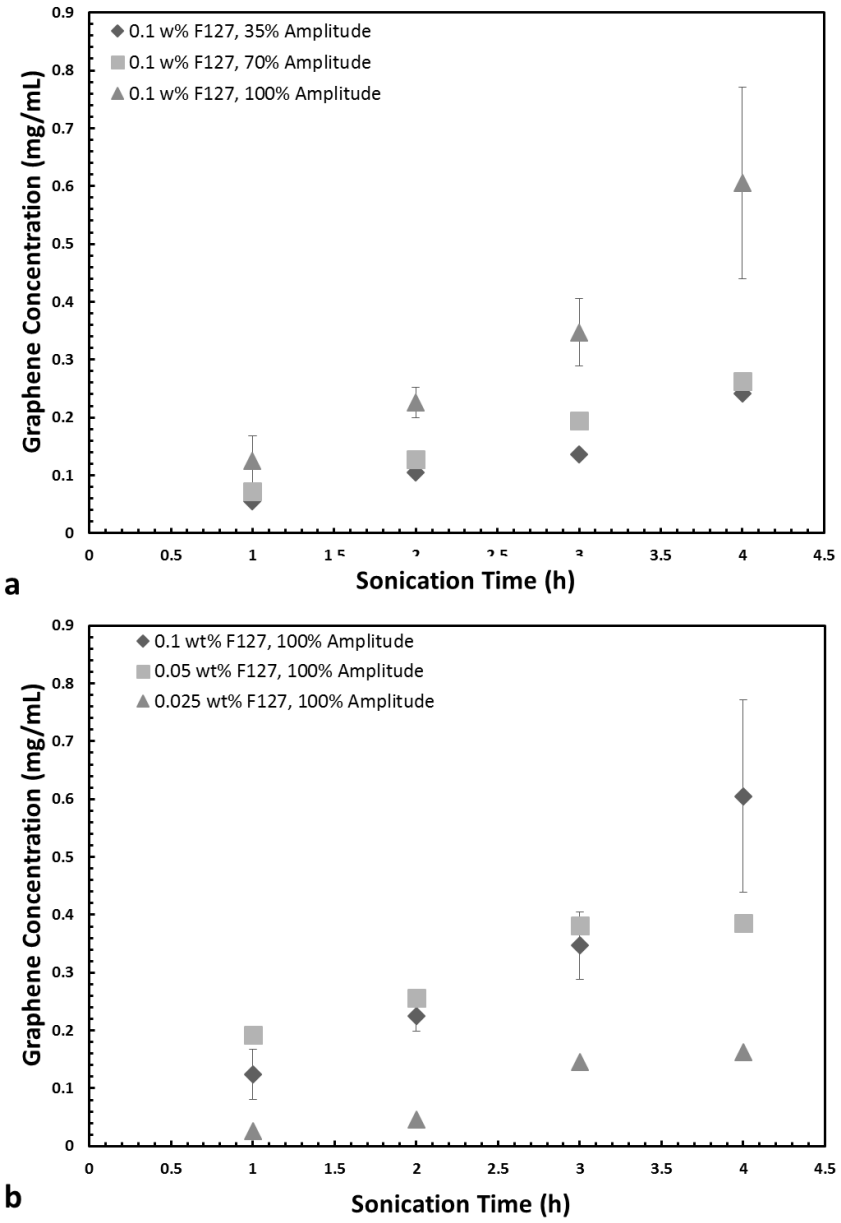

Figure B.2: Graphene concentration as a function of surfactant concentration below CMC. (a) Varying surfactant concentrations. (b) Varying amplitudes.

At the low surfactant concentrations, below CMC, shown in Figure B.2, sequential addition exfoliations could achieve graphene concentrations up to 0.61 mg/mL at a surfactant concentration of 0.1 wt%. However, increasing the surfactant concentration to above CMC

produced concentrations up to 5.51 mg/mL (Figure B.3). Recall that in batch systems (Chapter 3), the graphene concentration was 3.01 mg/mL, obtained in 4 h. Through extrapolation, the batch system would reach the same plateau of 5.51 mg/mL after 7 h of continuous sonication.

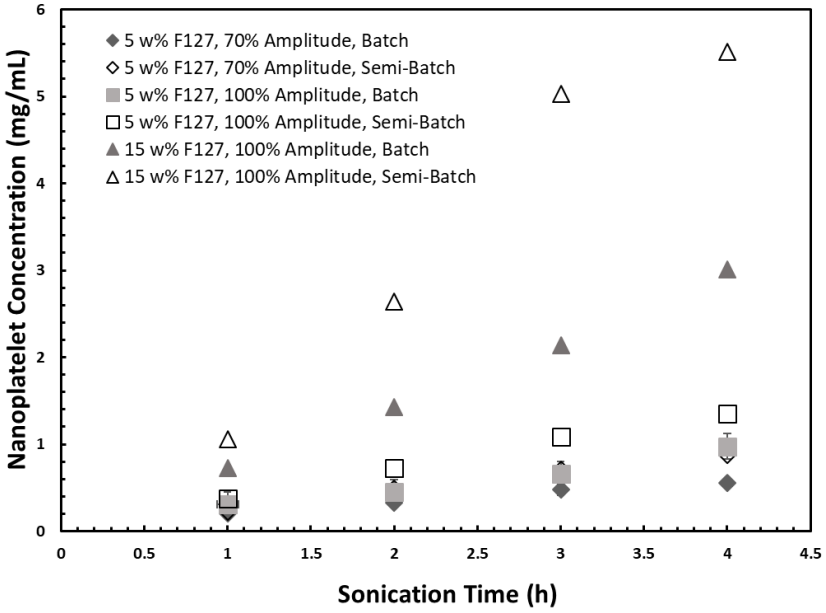

Figure B.3: Comparison between batch and sequential addition systems above CMC.

These results demonstrate that the sequential addition may be more effective in producing higher graphene nanoplatelet concentrations at shorter processing times. This suggests that constantly replenishing the surfactant available in the dispersion may be more effective in stabilizing the GNPs that are produced during sonication. It should be noted that the initial volume of the exfoliating sample in sequential addition conditions is lower, thereby providing a larger power density to the system.

At lower surfactant concentrations, the particle size, as measured by DLS, is not affected by the type of sonication system (Figure B.4). At each hour interval, the particle sizes remain constant, between 200-400 nm for both sequential addition and batch systems. Similar to batch systems,

neither the sonication time nor the amplitude change the measured particle size. However, at higher surfactant concentration, the particle size is dependent on the type of sonication system. Sequential addition systems produced smaller particle sizes (approximately 350 nm) which were closer to what was measured at surfactant concentrations of 10 wt% in batch systems. Table B.2 displays the average particle size and particle size distribution.

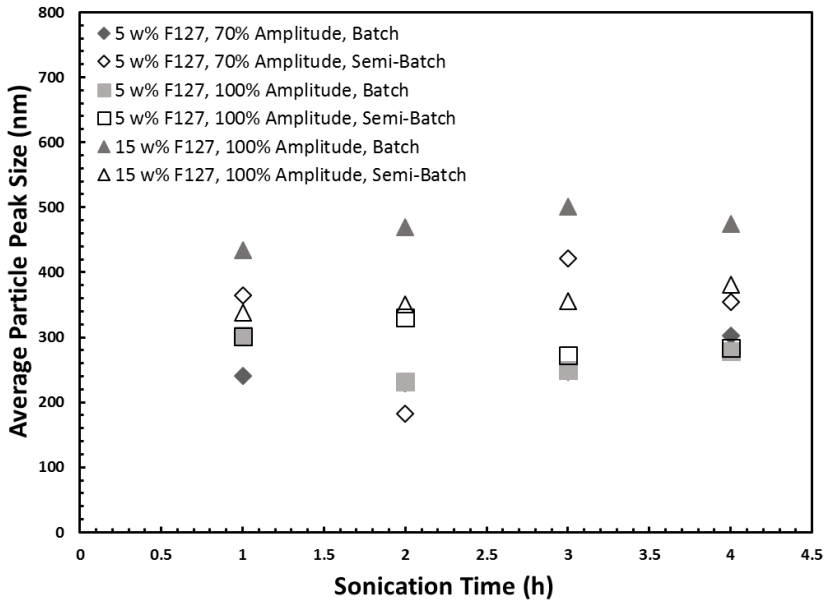

Figure B.4: Comparison of the average peak particle sizes between batch and sequential addition systems.

Table B.2: Effect of surfactant concentration on the average particle size (based on the 4 hourly samples in Figure B.4) and polydispersity index.

Exfoliation Condition	Average Particle Size (nm)	PdI
5 wt% F127, 70% amplitude, Batch	255	0.270
5 wt% F127, 70% amplitude, Sequential addition	331	0.195
5 wt% F127, 100% amplitude, Batch	266	0.174
5 wt% F127, 100% amplitude, Sequential addition	297	0.165
15 wt% F127, 100% amplitude, Batch	470	0.031
15 wt% F127, 100% amplitude, Sequential addition	357	0.066

B.4 Conclusion

Sequential addition of surfactant generates higher graphene nanoplatelet concentrations (5.51 $mg \cdot mL^{-1}$) compared to batch systems (3.01 $mg \cdot mL^{-1}$). The average particle size and particle size distribution was not significantly affected by the sonication conditions and the surfactant concentration. The sequential addition provides a promising route to achieve higher GNP yields, without suffering from complications due to high viscosity, and should therefore merits further investigation.

Appendix C: Extinction Coefficient

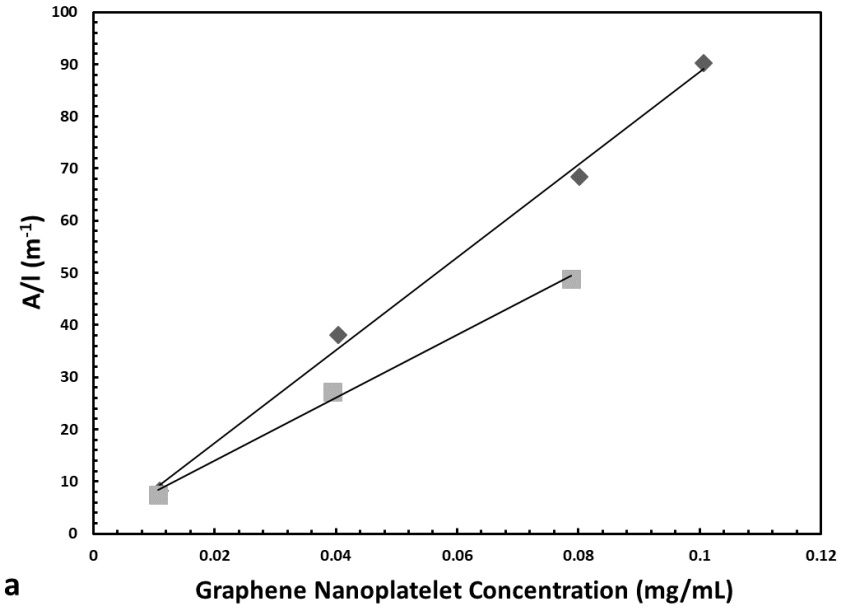

Figure C.1: Extinction coefficient determined using a known volume of GNP solution and the subsequent dry mass of GNPs from the same dispersion.

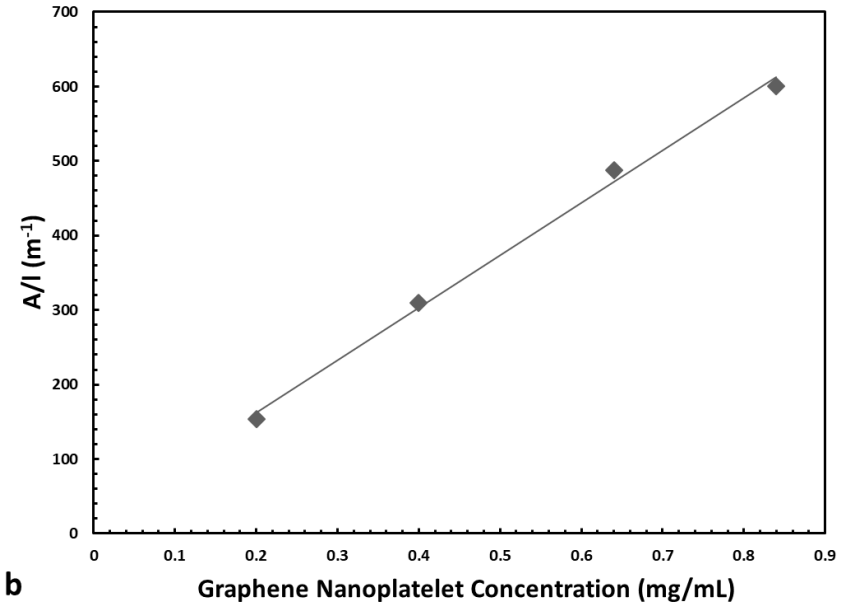

Figure C.2: Extinction coefficient determined using a known mass of GNPs and dispersing into known volume of NMP.

Appendix D: Dimensional Analysis

D.1 Ultrasonication

Five parameters were considered to describe the performance of the system: exfoliated graphite concentration (C), initial graphite concentration (C_i), sonication time (t), power density based on digital output on the sonicator (P), and solution volume (V). Thus, there are 5 variables and 3 dimensions present in the dimensional analysis. Two dimensionless terms were generated using the Buckingham Π theorem where C_i, t, and V were selected as repeating variables: $\Pi_1 = C \cdot C_i^{-1}$, and $\Pi_2 = P \cdot t^3 \cdot C_i \cdot V^{-5/3}$. These terms were used to develop a relationship between C, Ci, t, P, and V: $C \sim P \cdot t^3 \cdot V^{-5/3}$.

D.2 Shear Exfoliation

There are 6 variables and 3 dimensions present in the dimensional analysis using the Buckingham Π theorem. The three repeating variables that were selected were C_i, t, and D where 3 dimensionless terms (Π_1, Π_2, and Π_3) were generated: $\Pi_1 = C \cdot C_i^{-1}$, $\Pi_2 = V \cdot D^{-3}$, and $\Pi_3 = N \cdot t$. Combining the dimensionless terms provides a relationship between C, Ci, t, N, D, and V: $C \sim C_i \cdot V \cdot N \cdot t \cdot D^{-3}$. However, in the set of experiments the initial graphite concentration, rotor diameter, and solution volume were kept constant, thereby reducing the relationship to $C \sim N \cdot t$.

Appendix E: Particle Size Distribution for Ultrasonication, obtained by DLS

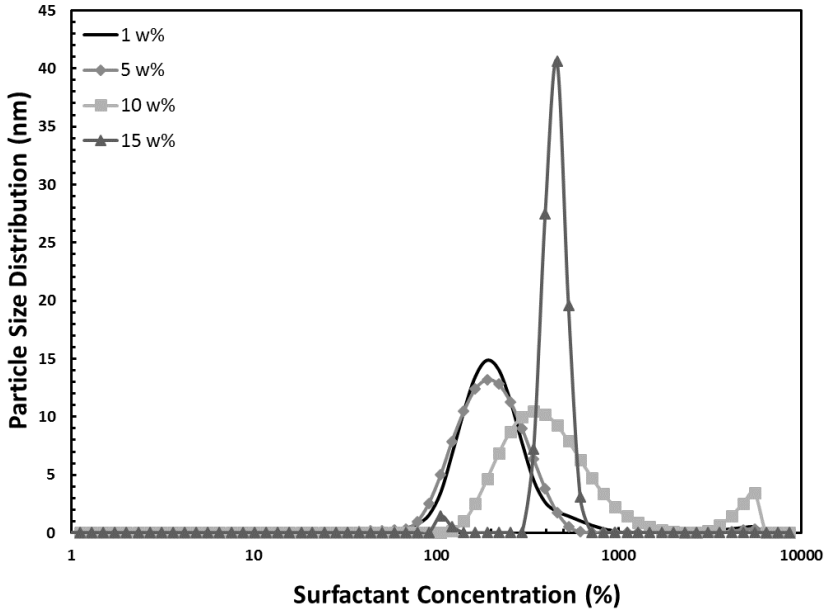

Figure E.1: GNP Particle size distribution obtained by ultrasonication in the presence of Pluronic® F127 at t=4 h, as a function of surfactant concentration at 100% amplitude.

Appendix F: Particle Size Distribution for Shear Exfoliation, obtained by DLS

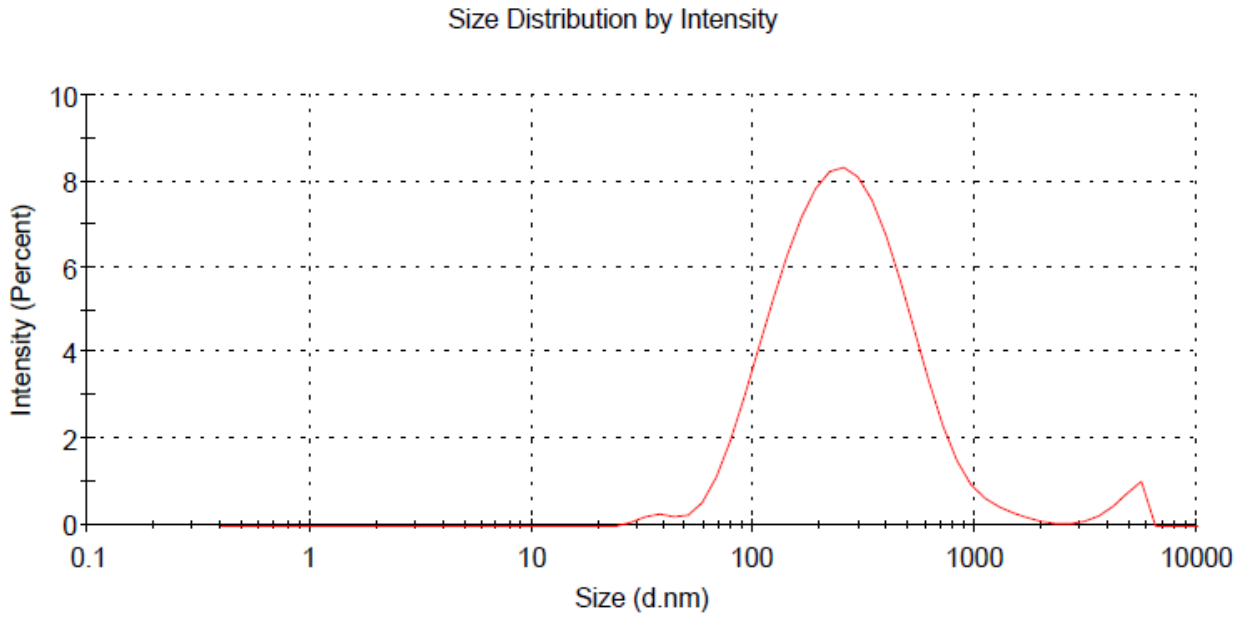

Figure F.1: GNP Particle size distribution at 1 wt% surfactant concentration in a shear exfoliation system (t=60 min, 6000 rpm).

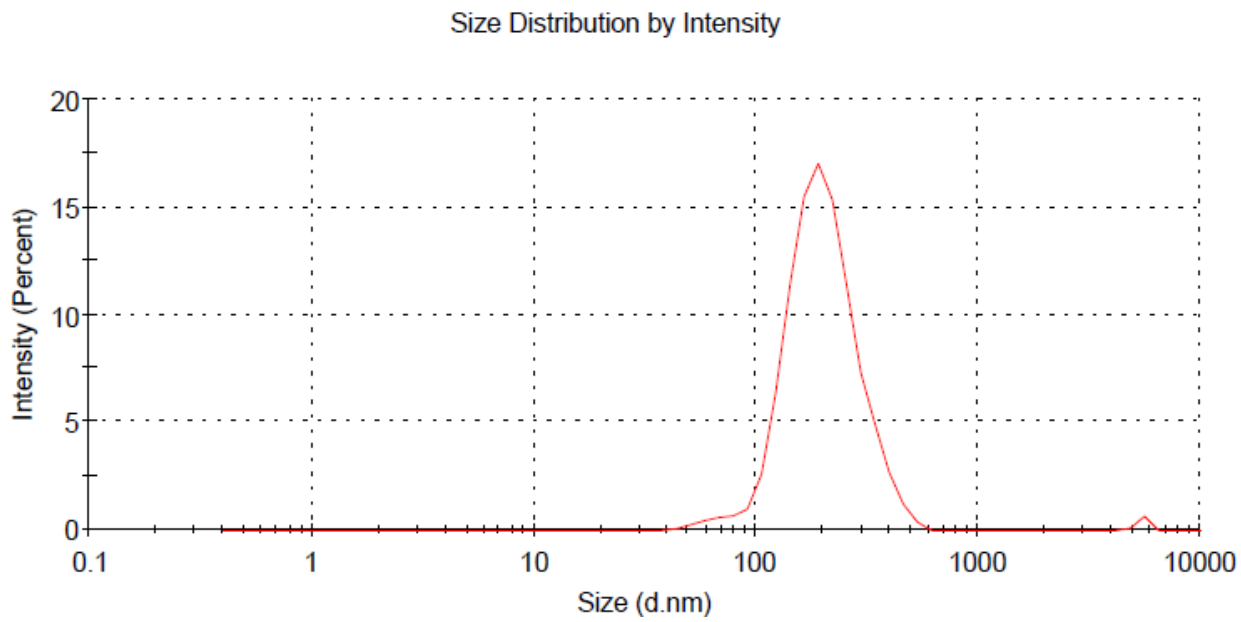

Figure F.2: GNP Particle size distribution at 5 wt% surfactant concentration in a shear exfoliation system (t=60 min, 6000 rpm).

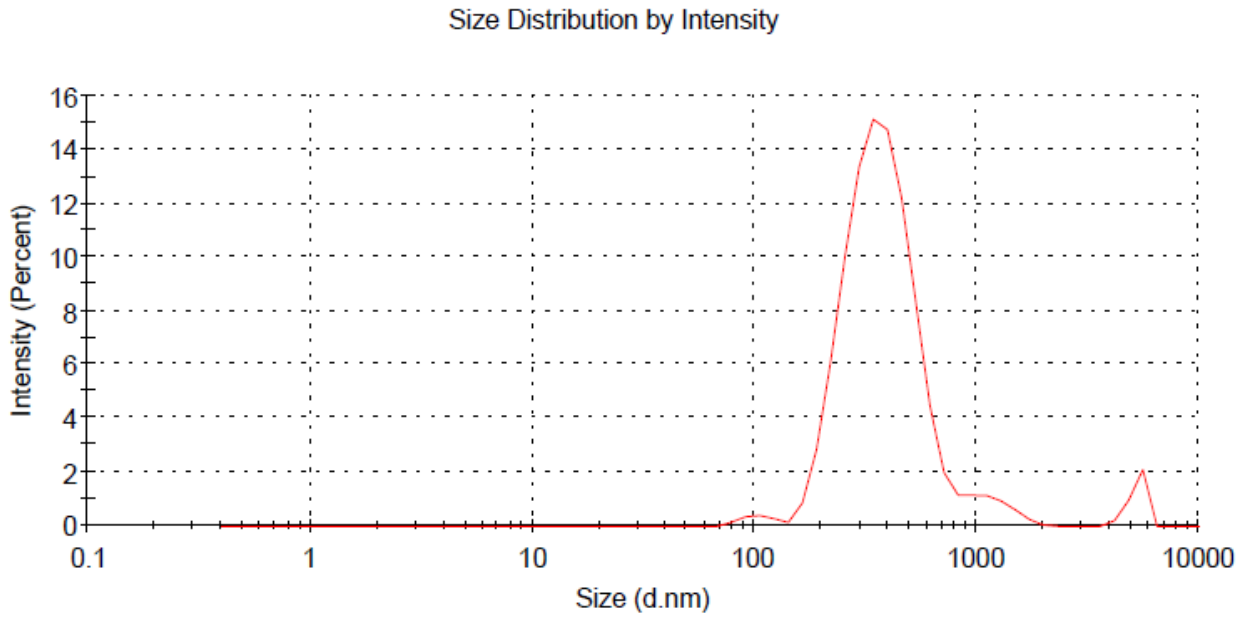

Figure F.3: GNP Particle size distribution at 10 wt% surfactant concentration in a shear exfoliation system (t=60 min, 6000 rpm).